Distribution of platinum-group and chalcophile elements in the Aguablanca Ni–Cu sulfide deposit (SW Spain): Evidence from a LA-ICP-MS study

R. Piña [a,*], F. Gervilla [b], S.-J. Barnes [c], L. Ortega [a], R. Lunar [a]

[a] Facultad de Geología, Universidad Complutense de Madrid, Madrid, Spain
[b] Facultad de Ciencias, Universidad de Granada-CSIC, Granada, Spain
[c] Sciences de la Terre, Université du Québec à Chicoutimi, Saguenay, Québec, Canada

Keywords:
Platinum-group elements
Aguablanca
Laser ablation
Base-metal sulfides
Pyrite

A B S T R A C T

The concentrations of platinum-group elements (PGE) and chalcophile elements Ni, Co, Au, Ag, Se, Re, Cd, Bi, Te and As have been determined by laser ablation-inductively coupled plasma-mass spectrometry (LA-ICP-MS) in base metal sulfide minerals (BMS) from the Aguablanca Ni–Cu deposit, SW Spain. The main aim was to constrain the role played by the BMS as hosts of PGE as this reveals important information regarding the processes controlling the distribution of these elements in the deposit. The BMS (pyrrhotite, pentlandite, chalcopyrite and minor pyrite) occur as semi-massive, disseminated and minor chalcopyrite-veined ores. On the basis of whole rock metal abundances and BMS mineralogy, these ore types have been interpreted to be the result of the fractionation and crystallization of an immiscible sulfide liquid.

Platinum-group and chalcophile element concentrations vary as a function of the BMS and ore types. The partitioning behavior of some of these metals during the fractional crystallization of the sulfide liquid largely governed their distribution in the ore. Rhenium, Os, Ir, Ru, and Rh occur mostly in solid solution in pyrrhotite and pentlandite from the semi-massive ore which has been interpreted to represent monosulfide solid solution (*mss*) cumulates. The *mss* crystallization gave rise to minor Cu-rich sulfide liquid in the form of chalcopyrite veinlets with relatively Pd-, Au- and Ag-enriched chalcopyrite, and minor Re-, IPGE- and Rh-depleted pyrrhotite and pentlandite. Platinum-group element contents in the BMS from the disseminated ore, interpreted to represent an original unfractionated sulfide melt, are approximately intermediate to the semi-massive and chalcopyrite-veined ores.

Palladium and Pt occur mostly associated with Bi, Te, and As forming platinum-group minerals (PGM, Pd–Pt bismuthotellurides and Pt arsenides) within individual BMS grains. This preferential location along with the textures adopted (usually rounded grains and laths) and the temperatures of crystallization (inferred below 500 °C) suggests that Pd and Pt, initially dissolved in the BMS, were exsolved along with Bi, Te and As to form the PGM assemblage present in the ore. Some Pd (approximately 30% of the bulk) remains in solid solution in pentlandite for the three ore types. The presence of Pd in pentlandite is likely a combined effect of limited sulfide fractionation with some of Pd remaining in *mss* and Pd diffusion into pentlandite from the *mss* and Cu-rich portions on cooling.

Two textural types of pyrite hosting distinct PGE concentrations have been described: (1) large idiomorphic pyrite and (2) ribbon-like pyrite. Idiomorphic pyrite is the unique BMS hosting Pt (with contents as high as 15 ppm) and also contains relatively high Rh concentrations (4–31 ppm). By contrast, ribbon-like pyrite has no Pt and hosts similar Os, Ir, Ru and Rh concentrations (30–360 ppb) to those of the host pyrrhotite to that it replaces. The origin of the idiomorphic grains, whether exsolution products from *mss* or alteration products of pyrrhotite, is not well known and further work will be necessary to constrain this point. Nevertheless, the presence of PGE hosted by pyrite reveals that this sulfide should not be overlooked as a potential carrier of PGE in Ni–Cu–(PGE) ore deposits.

1. Introduction

The Aguablanca deposit (SW Spain) is a Ni–Cu–platinum-group element (PGE) ore deposit which contains 15.7 million tons (Mt), grading 0.66 wt.% Ni, 0.46 wt.% Cu and 0.47 g/t PGE (Tornos et al., 2001; Ortega et al., 2004; Lunar et al., 2008; Piña et al., 2006, 2008, 2010). The sulfide mineralization occurs in the form of three ore

* Corresponding author.
E-mail address: rpinagar@geo.ucm.es (R. Piña).

types: semi-massive, disseminated and minor chalcopyrite-veined ore. These ore types are the result of the fractionation and crystallization of an immiscible sulfide liquid segregated from a mafic silicate melt, after reaching sulfide saturation by assimilation of crustal sulfur (Ortega et al., 2004; Piña et al., 2008, 2010). In this way, the semi-massive ore has been interpreted to represent monosulfide solid solution (*mss*) cumulates, the chalcopyrite veinlets likely formed by crystallization of Cu-rich residual sulfide liquid, and the disseminated ore probably represents in-situ crystallization of an original sulfide melt.

Most of what is known on the distribution of the PGE in the Aguablanca ore has been summarized by Ortega et al. (2004) and Piña et al. (2008). Based on the whole rock PGE abundances and PGE mineralogy, these studies concluded that PGE distribution is mainly governed by base metal sulfides (BMS) such as pyrrhotite, pentlandite and chalcopyrite. The PGE were originally collected by the immiscible sulfide melt due to their high partition coefficients between sulfide and silicate liquid (10^3–10^5, Peach et al., 1990; Fleet et al., 1991; Crocket et al., 1992) and were later partitioned between the three ore types during sulfide fractionation. However, little is known about the precise location of these elements and the processes that have controlled their distribution in the deposit. The ore contains a platinum-group mineral (PGM) assemblage consisting of mostly Pd–Pt–Bi–Te bearing phases and sperrylite $PtAs_2$, however these minerals do not seem to be abundant enough to account for the observed whole-rock concentrations. This is especially evident for the Ir-group elements (IPGE, Os, Ir and Ru) and Rh, because very few PGM comprising these elements have been identified, and therefore their distribution must be controlled by other phases rather than PGM. In absence of PGM, BMS can be an important host of PGE (e.g., Noril'sk, Russia, Bushveld Complex, South Africa, and Great Dyke, Zimbabwe, Barnes et al., 2008), but in Aguablanca this possibility has not yet been assessed due to the lack of data on the PGE contents of the BMS.

To investigate the precise distribution of the PGE in the mineralization and the role played by the BMS as carriers of PGE, we have determined the concentrations of PGE and chalcophile elements, such as Ni, Co, Re, Au, Ag, Se, Cd, Te, Bi and As, in the BMS employing laser ablation inductively coupled plasma mass spectrometry (LA-ICP-MS). This technique has been successfully used to determine the PGE content in BMS of PGE-rich reefs (e.g., J-M Reef in the Stillwater Complex, Godel and Barnes, 2008; Merensky Reef and Platreef in the Bushveld Complex, Ballhaus and Sylvester, 2000; Godel et al., 2007, Holwell and McDonald, 2007, Hutchinson and McDonald, 2008), in PGE-rich Ni–Cu ores (e.g., Noril'sk, Cabri et al., 2003; Barnes et al., 2006) and in PGE-poor Ni–Cu ores (e.g., Copper Cliff and Creighton Mines in Sudbury, Huminicki et al., 2005 and Dare et al., 2010a, respectively). This work expands the detailed mineralogical and geochemical study of the Aguablanca deposit (Ortega et al., 2004; Piña et al., 2006, 2008) and it is the first attempt to establish which minerals host the PGE in the deposit. Furthermore, we discuss what processes were important in controlling the distribution of the PGE and chalcophile elements in the Aguablanca ore.

2. The Aguablanca Ni–Cu–(PGE) sulfide deposit

2.1. Geological background

The Ni–Cu ore occurs within the Aguablanca stock (Fig. 1). This is a small mafic intrusion (341 ± 1.5 Ma, U–Pb on magmatic zircons, Romeo et al., 2006) located in the northern part of the Santa Olalla Igneous Complex (SOIC). This complex consists of a calc-alkaline plutonic group situated in the southern limb of the Olivenza-Monesterio antiform, a major WNW–ESE trending Variscan structure occupying a central position within the Ossa-Morena zone (OMZ) of the Iberian Massif (Fig. 1). A detailed geological review of the Iberian Massif is given by Quesada (1991) and references therein. The SOIC intrudes Early Cambrian volcanic, volcanoclastic and carbonate rocks (Bodonal Cala

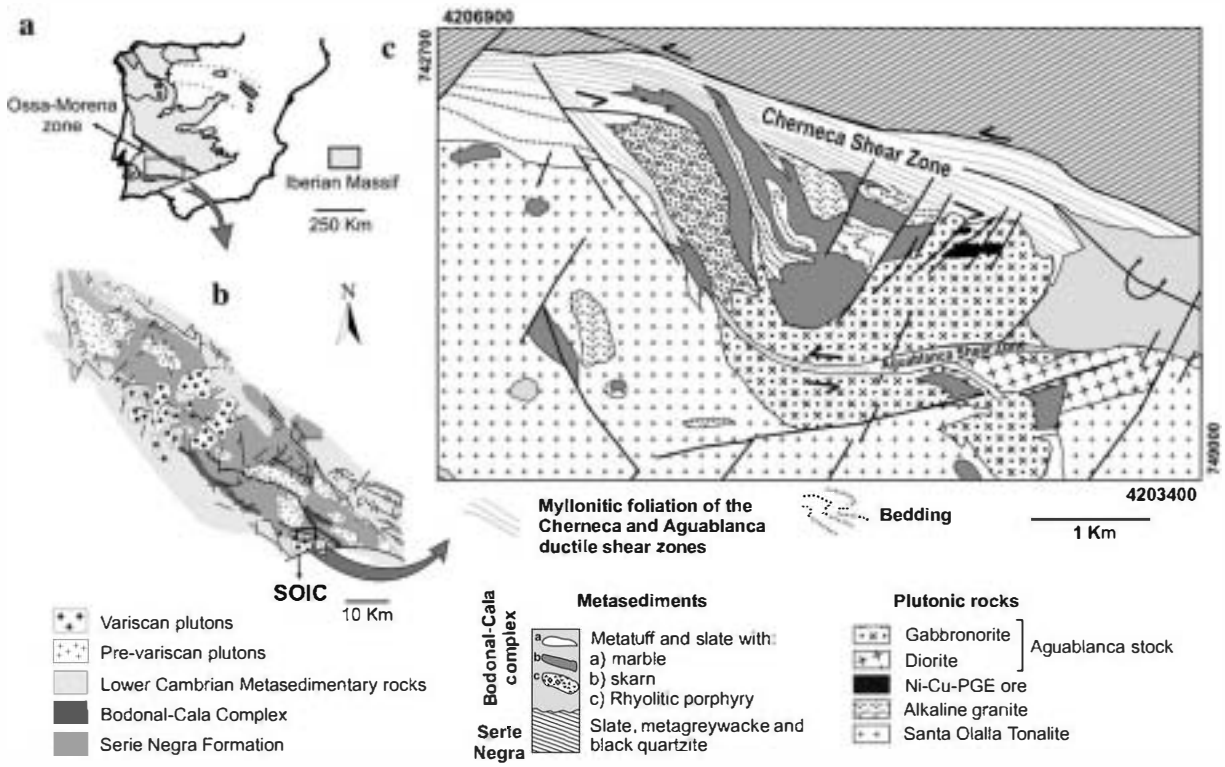

Fig. 1. (a) Location of the Ossa-Morena zone (OMZ) in the Iberian Massif. (b) Situation of the Santa Olalla Igneous Complex (SOIC) in the southern limb of the WNW–ESE trending Olivenza-Monesterio anticline. (c) Simplified geologic map of the Aguablanca stock showing the location of the Ni–Cu–(PGE) ore. The Cherneca and Aguablanca ductile shear zones are also shown. Modified from Piña et al. (2010).

Complex) that overlie Late Neoproterozoic metasedimentary rocks (Serie Negra Formation), mainly composed of graywackes and pyrite-rich black slates (Carvalhosa, 1965; Vegas, 1968). Radiometric ages and structural data suggest that the SOIC was emplaced during the transpressive Variscan orogeny in Early Carboniferous times (Tornos et al., 2001; Romeo et al., 2006, 2008). Based on structural and gravity analyses, Romeo et al. (2008) proposed that the Aguablanca stock was emplaced across a hundred-meter-scale, open tensional fracture developed under the sinistral strike-slip ductile strain regime in the area between the Cherneca and Aguablanca shear zones (Fig. 1).

The northern part of the Aguablanca stock hosts the Ni–Cu sulfide mineralization. In this part, rocks comprise mostly medium- to coarse-grained cumulate-textured hornblende-bearing gabbronorite and gabbro (Piña et al., 2006). Orthopyroxene, clinopyroxene and plagioclase are cumulus phases, whereas the interstitial material is green-brown amphibole, phlogopite and minor quartz. Locally, rocks are pyroxenites and olivine-bearing gabbronorites. Magmatic foliations defined by tabular plagioclase crystals are commonly concentric with respect to the intrusion boundaries. The Aguablanca stock underwent a locally very intense, pervasive retrograde alteration. Cumulate textures are partially obliterated by a secondary mineral assemblage formed by hydrothermal alteration and/or low-grade greenschist metamorphism. Clinopyroxene is variably altered to actinolite and chlorite, being locally completely replaced. Orthopyroxene is generally less altered but is also partially replaced by bastite, actinolite and talc. Plagioclase is irregularly altered to sericite, epidote–zoisite group minerals, chlorite and carbonates.

The Ni–Cu ore occurs as a subvertical (dipping 70–80°N), funnel-like magmatic breccia (250–300 m wide N–S, up to 600 m long E–W and 600 m deep) composed of rocks containing semi-massive and disseminated sulfides, which host variable amounts of randomly distributed unmineralized, mafic–ultramafic fragments. The mineralized breccia exhibits a concentric structure made up of an inner core of semi-massive sulfide-bearing rocks surrounded by disseminated sulfide-bearing gabbronorite and minor gabbro and norite (hereafter semi-massive and disseminated ores, respectively). The disseminated ore grades outwards to sulfide-free rocks with gradational contacts. Small (<10 cm wide) chalcopyrite veinlets occur cross-cutting the semi-massive and disseminated ores as well as across fragments of the breccia. Fragments consist of different fine-to medium-grained, cumulate-textured rock-types (peridotite, pyroxenite, gabbro and anorthosite). These fragments have been interpreted to represent different stages of igneous cumulate formation, likely in an unexposed mafic–ultramafic (layered?) sequence situated beneath the Aguablanca stock (Piña et al., 2006). From mineralogical and geochemical data (i.e., Ni-depleted olivines and Cu/Zr whole rock ratios), these authors suggested the segregation of a sulfide liquid during the first stages of the differentiation of the cumulate sequence. Sulfur saturation was likely reached by local assimilation of crustal S from pyrite-rich black slates of the Neoproterozoic Serie Negra Formation, as indicated by the sulfur isotope compositions for pyrrhotite, pentlandite, and chalcopyrite ($\delta^{34}S = +7.4‰$, Casquet et al., 2001). Based on the existing information, two distinctive stages are established for the origin and emplacement of the deposit (Piña et al., 2010): (1) a scenario similar to most plutonic Ni–Cu sulfide ores including magma emplacement in the crust, assimilation of crustal S, and segregation and gravitational settling of immiscible sulfide melt, and (2) final emplacement of the Ni–Cu sulfide-bearing rocks by the upward brecciation of the sequence due to multiple melt injections controlled by successive opening events of tensional fractures related to the Cherneca ductile shear zone.

2.2. Ore mineralogy and textures

The ore mineralogy and textures, including PGE mineralogy, have been the focus of previous papers (Ortega et al., 2004; Piña et al., 2008) and only a brief review is presented here.

The semi-massive ore samples show a ground mass of Fe–Ni–Cu sulfides (from 20 to 70 vol.%) with early-crystallized idiomorphic silicates (mostly pyroxene, plagioclase and/or olivine). Pyrrhotite is the predominant BMS (34–77 modal %). It occurs commonly associated with pentlandite (11–34 modal %), which forms aggregates around or flames within pyrrhotite. Chalcopyrite (<11 modal %) forms anhedral grains of variable size, and magnetite and ilmenite (up to 2 modal %) are present as isolated crystals generally within pyrrhotite. Pentlandite/chalcopyrite ratios are commonly above 4. In the disseminated ore, BMS (<20 vol.%) occur as polymineralic aggregates, randomly and interstitially distributed between silicate grains. These rocks mostly consist of medium-grained hornblende-bearing gabbronorite with minor gabbro, norite and pyroxenite. In comparison to the semi-massive ore, the disseminated ore has higher amounts of chalcopyrite (12–58 modal %) and lower pentlandite (3–18 modal %) with pentlandite/chalcopyrite ratios commonly below 1. Pyrrhotite is the most abundant sulfide (21–68 modal %). The chalcopyrite veinlets are mostly made up of massive chalcopyrite with minor amounts of anhedral pyrrhotite and pentlandite. Locally, chalcopyrite includes subhedral grains of an Ag–Fe–Ni sulfide (probably, argentopentlandite).

Pyrite can be locally abundant, up to 10 modal % of the total sulfides. It mostly occurs as large euhedral crystals and as ribbon-like aggregates outlining the curved lamellae of monoclinic pyrrhotite in the semi-massive ore. From textural features and cross-cutting relationships, Ortega et al. (2004) suggested that the euhedral pyrite formed early in the postmagmatic history of the deposit (prior to and/or coevally with the exsolution of the coarse-grained pentlandite) and predates the precipitation of the ribbon-like aggregates. However, the origin of these pyrites, whether primary/magmatic or hydrothermal, is not well established yet.

The PGM assemblage consists, in a decreasing order of abundance, of merenskyite ($PdTe_2$), palladian melonite ($NiTe_2$), michenerite (PdBiTe), moncheite ($PtTe_2$) and sperrylite ($PtAs_2$) (Ortega et al., 2004; Piña et al., 2008; Suárez et al., 2010). Other minor phases comprise Os–Ir–As–S, Ir–As–S and Ir–Pt–As. The predominance of Bi–Te-bearing PGMs over As-bearing PGMs occurs invariably in the three ore types. Platinum-group minerals are significantly more abundant in the semi-massive (70.8% of a total of 301 identified grains) and chalcopyrite veined (21.2%) ores than in the disseminated ore (8%). The PGM are spatially associated with BMS. They occur included in sulfides (76%), along sulfide–silicate (11%) and sulfide–sulfide (6%) boundaries, and only few of them are included in silicates (7%). Based on textural relationships and composition of these phases (Bi-rich merenskyite and michenerite form at temperatures <600 °C Hoffman and MacLean, 1976), Piña et al. (2008) concluded that Pd and Pt, initially dissolved in the BMS, exsolved at low temperatures to form the Pd–Pt bismuthotellurides and Pt-arsenides.

3. Analytical method

We studied 5 representative samples from semi-massive ore, 3 from disseminated ore and 1 chalcopyrite veinlet. Firstly, pyrrhotite, pentlandite, chalcopyrite, and pyrite were analyzed for major elements (S, Fe, Ni and Cu) at the Electron Microscope Centre of the University Complutense of Madrid, using a JEOL JXA-8900 M electron microprobe (Table 1). The accelerating voltage was 20 kV, the beam current 50 nA, the beam diameter 1–5 μm and the counting period ranged from 20 to 60 s. Galena (PbS) for S and pure metals for Ni, Fe and Cu were used as standards.

The BMS were later examined on polished sections by optical microscope and sites for laser ablation analyses were selected. Sulfides were then analyzed using laser ablation inductively-coupled plasma mass spectrometry (LA-ICP-MS) at Université du Quebec a Chicoutimi (UQAC), Canada. The following isotopes were monitored ^{29}Si, ^{33}S, ^{34}S, ^{44}Ca, ^{47}Ti, ^{54}Fe, ^{55}Mn, ^{57}Fe, ^{58}Fe, ^{59}Co, ^{60}Ni, ^{61}Ni, ^{63}Cu, ^{65}Cu, ^{66}Zn, ^{68}Zn, ^{75}As, ^{77}Se, ^{82}Se, ^{95}Mo, ^{99}Ru, ^{100}Ru, ^{101}Ru, ^{102}Ru, ^{103}Rh,

Table 1
Average of the Fe, Ni, Cu and S concentrations in the BMS as a function of the ore type.

Ore-type	BMS mineral	*n*	S	Ni	Cu	Fe	Total
			wt.%	wt.%	wt.%	wt.%	wt.%
Semi-massive	Pyrrhotite	49	40.75	0.62	<0.1	57.43	98.80
	Pentlandite	52	34.22	35.65	<0.1	28.75	98.62
	Pentandite — flames	10	34.29	36.10	<0.1	29.50	99.89
	Chalcopyrite	16	35.87	<0.1	34.30	29.27	99.44
	Pyrite	16	52.27	1.50	<0.1	45.01	98.78
Disseminated	Pyrrhotite	45	40.46	0.65	<0.1	57.99	99.10
	Pentlandite	24	34.16	35.39	<0.1	29.11	98.66
	Chalcopyrite	23	35.79	<0.1	34.07	29.86	99.72
Chalcopyrite veinlets	Pyrrhotite	5	40.77	1.02	<0.1	56.94	98.73
	Pentlandite	3	33.92	35.49	<0.1	27.25	96.66
	Chalcopyrite	11	35.71	<0.1	34.31	29.11	99.13

n: number of grains analyzed.

^{105}Pd, ^{106}Pd, ^{107}Ag, ^{108}Pd, ^{109}Ag, ^{111}Cd, ^{118}Sn, ^{121}Sb, ^{125}Te, ^{126}Te, ^{128}Te, ^{185}Re, ^{187}Re, ^{189}Os, ^{190}Os, ^{191}Ir, ^{193}Ir, ^{194}Pt, ^{195}Pt, ^{197}Au, ^{208}Pb, and ^{209}Bi. The purpose of monitoring Si, Ca, Ti and Mn was to ensure that no silicates, carbonates or oxides were included in the analyses. The purpose of monitoring S, As, Sb, Sn, Te and Bi was to screen the spectra for platinum-group minerals. ^{61}Ni, ^{63}Cu, ^{65}Cu, ^{66}Zn, ^{68}Zn and ^{111}Cd were used to correct for interferences on ^{101}Ru, ^{103}Rh, ^{105}Pd, ^{106}Pd and ^{108}Pd. Multiple isotopes of each element were collected to check for unforeseen interferences. The isotopes used to determine the element concentrations were ^{59}Co, ^{61}Ni, ^{75}As, ^{82}Se, ^{101}Ru, ^{103}Rh, ^{105}Pd, ^{107}Ag, ^{108} Pd, ^{111}Cd, ^{125}Te, ^{185}Re, ^{189}Os, ^{191}Ir, ^{195}Pt, ^{197}Au and ^{209}Bi. The UQAC laser ablation ICP-MS consists of a Thermo X7 mass spectrometer with a high-performance interface coupled to a New Wave Research 213 nm Nd:YAG UV laser ablation microprobe. A beam of 80 μm diameter, a laser frequency of 10 Hz and a power of 0.8 mJ/pulse were used. The gas blank was measured for 20 s before switching on the laser for 60 s. An argon–helium gas mix was used as carrier gas. The material was then analyzed using the Thermo X7 ICP-MS operating in time resolved mode using peak jumping and a dwell time of 10 ms/peak per element. Internal standardization was based on ^{57}Fe employing mean Fe values for each BMS determined by the electron microprobe (Table 1). Data reduction was carried out using PlasmaLab software (ThermoElemental) by subtracting gas background from each of the analyzed isotopes. To calibrate for PGE and Au, we used the certified reference material Laflamme Po727, provided by the Memorial University of Newfoundland, which is a synthetic FeS doped with ~40 ppm of each PGE and Au (Table 2a). For Co, As, Se, Ag, Cd and Bi, the certified reference material MASS-1, a ZnCuFeS pressed powder pellet provided by the National Institute for Standards and Technology (NIST) and doped with 50–70 ppm of each element, was used (Table 2a). The calibrations were monitored using two in-house reference materials: Po-62, an FeS doped with ~2 ppm PGE, Au and Re, made by Dr. Peredoegova in the McGill University and JB-mss-5 which is a synthetic FeS doped with 50–80 ppm chalcophile elements, provided by Prof. Brenan of the University of Toronto (Table 2b). JB-mss-5 was also used to calibrate for Ni and Re as neither of the certified materials contained these elements. Tellurium was determined using the semi-quantitative option of PlasmaLab software. The semi-quantification mode uses the sensitivity of the isotopes which are quantified to draw a curve of isotopic number versus sensitivity. The isotope for which there is no reference material is then projected onto this line and the sensitivity is estimated from this. The reliability of the result depends on: a) how well the isotopes close to the uncalibrated isotope are determined; and b) the isotope not fractionating from the isotopes used to draw the calibration curve. In our experience in semi-quantitative mode provided the sensitivity for the isotopes close to the element is well known the results are generally within ~40% of the quantitative determinations.

Table 2a
Reference materials and values used to calibrate the laser.

Isotope	^{59}Co	^{61}Ni	^{75}As	^{82}Se	^{101}Ru	^{103}Rh	^{105}Pd	^{107}Ag	^{108}Pd	^{111}Cd	^{125}Te	^{185}Re	^{189}Os	^{193}Ir	^{195}Pt	^{197}Au	^{209}Bi
	ppm	ppm	ppm	ppm	ppm	ppm	ppm	ppm	ppm	ppm	ppm	ppm	ppm	ppm	ppm	ppm	ppm
Ref. material	Mass-1	JB-mss-5	Mass-1	Mass-1	po-727	po-727	po-727	Mass-1	po-727	Mass-1	Mass-1	JB-mss-5	po-727	po-727	po-727	po-727	Mass-1
Based on	Wilson et al. (2002)	AA-sol	Wilson et al. (2002)	Wilson et al. (2002)	Certificate	Certificate	Certificate	Wilson et al. (2002)	Certificate	Wilson et al. (2002)	LA-semiquant	ID-ICP-MS	Certificate	Certificate	Certificate	Certificate	LA-NIST-610
Value	67	10,487	65	53	36.26	41.62	43.05	67	43.82	70	33	20.7	46.85	47.81	35.37	45.79	66

Table 2b
Results for in-house reference materials used as monitors.

Po-62																				
Working values					1.43	1.25	1.6			1.56			0.49	1.50	1.53	1.64	1.56			
stdev																				
Based on					0.05	0.02	0.13			0.19			0.01	0.27	0.04	0.13	0.01			
					ID-ICP-MS	sol-ICP-MS	ID-ICP-MS			ID-ICP-MS			ID-ICP-MS	ID-ICP-MS	ID-ICP-MS	ID-ICP-MS	sol-ICP-MS			
This run n = 12					1.36	1.08	1.20			1.27			0.42	1.68	1.57	1.52	1.20			
stdev					0.10	0.03	0.29			0.26			0.03	0.09	0.08	0.49	0.36			
JB-mss-5																				
Working values	0.28	10.467	63	48.35	21.72	61.4	64.1	53.0	61.40	0.13	66	20.7	42.5	43.98	39.9	35.9	76.1			
stdev	0.02		10	34.60	0.42	7.2	1.28	4.9	1.28	0.04	11	0.41	0.28	1.32	1	4.8	2.9			
Based on	LA-NIST-610	AA-sol	LA-NIST-610	LA-NIST-610	ID-ICP-MS	sol-ICP-MS	ID-ICP-MS	sol-ICP-MS	ID-ICP-MS	LA-NIST-610	LA-semiquant	ID-ICP-MS	sol-ICP-MS	ID-ICP-MS	sol-ICP-MS	sol-ICP-MS	sol-ICP-MS			
This run n = 14		Used to calibrate	58.4	52.60	21.36	59.40	54.05	54.20	54.05	0.11	69.00	Used to calibrate	60.10	41.73	38.20	34.05	71.80			
stdev			2.1	8.00	1.30	2.50	1.80	1.70	1.90	0.06	8.00		8.30	3.70	3.90	3.34	5.50			

Mass-1 (FeCu2nS pressed powder pellet supplied by National Institute for Standards and Technology; JB-mss-5 synthetic FeS in house reference material; po-727 certified synthetic FeS supplied by the Memorial University of Newfoundland; po-62 synthetic FeS in house reference material. LA: semi quant = laser ablation using the semi-quantitative mode and LA-NIST-610 = laser ablation using NIST-610 to calibrate.

^{101}Ru was corrected for ^{61}Ni interference by using a NiS blank run at the beginning of each analytical session. ^{103}Rh and ^{105}Pd were corrected for $^{63}Cu^{40}Ar$ and $^{65}Cu^{40}Ar$, respectively, by running a (CuFe)S blank at the beginning of each session. In chalcopyrite, the interference of Cu argide on ^{103}Rh was so large that no Rh results can be reported for this mineral. ^{105}Pd was used for pyrrhotite and pentlandite analyses, but in chalcopyrite to avoid the $^{65}Cu^{40}Ar$ interference, ^{108}Pd was used. ^{108}Pd was corrected for any ^{108}Cd or $^{68}Zn^{40}Ar$ interference by monitoring ^{111}Cd and ^{68}Zn. Detection limits for laser analyses of the BMS were calculated using background counts for the gas blank and each BMS. The ranges, average and standard deviation of the concentrations of each element as a function of the ore type and BMS are summarized in Table 3. Tables with the individual analyses for each BMS are provided as supplementary electronic information (Tables S1, S2, S3 and S4). In the next section, we first describe the results obtained for pyrrhotite, pentlandite, and chalcopyrite, and later for pyrite since its trace metal abundances are significantly different to those.

4. Laser ablation ICP-MS results

4.1. Pyrrhotite, pentlandite and chalcopyrite

Platinum-group element concentrations vary as a function of the BMS and the ore type. Pentlandite is the principal BMS hosting PGE with values ranging from 578 to 7135 ppb. For any given sample, more than 85% of the PGE found in BMS occur in pentlandite. Most pyrrhotite grains have <400 ppb PGE (some grains containing up to 925 ppb), and chalcopyrite hosts the lowest PGE concentrations (most results are below 250 ppb). Overall, BMS from the semi-massive ore have higher PGE contents than those from the disseminated and chalcopyrite-veined ores (Table 3), due mainly to the high concentrations of Os, Ir, Ru, and Rh in pyrrhotite and pentlandite from semi-massive ore samples.

Osmium and Ir contents are positively correlated (Fig. 2a), as has been observed in similar studies at other Ni–Cu–PGE deposits (e.g., Merensky Reef in the Bushveld Complex, Godel et al., 2007; J-M Reef in the Stillwater Complex, Godel and Barnes, 2008). These elements are preferentially concentrated in pyrrhotite (16–189 ppb Os and 43–314 ppb Ir) and pentlandite (24–152 ppb Os and 47–259 ppb Ir) from the semi-massive ore (Fig. 3a and b). Flame-textured pentlandite has Os and Ir values (33–125 ppb Os and 61–244 ppb Ir) covering a similar range to the granular pentlandite (Table 3). In the disseminated ore, Os and Ir contents are lower to 40 and 45 ppb respectively for pyrrhotite, and 36 and 22 ppb respectively for pentlandite. These elements are below the detection limit, ~4–7 ppb, in all of the BMS from the chalcopyrite veinlet. Osmium and Ir in chalcopyrite are also below the detection limit (~7–10 ppb) in all ore types. An exception to this is some minor chalcopyrite from the semi-massive ore containing up to 87 ppb Os and 13 ppb Ir. Rhenium is relatively well correlated with Ir (Fig. 2b) and Os, and presents higher concentrations in pyrrhotite (from ~0.20 to 1.2 ppm, usually <0.5 ppm), pentlandite (from ~0.10 to 0.44 ppm) and chalcopyrite (up to 0.5 ppm) from the semi-massive ore than in these BMS from the disseminated ore (usually <0.15 ppm) (Fig. 2b). Rhenium is below the detection limit (~0.005 ppm) in all of the analyses from the chalcopyrite veinlet.

Ruthenium and Rh follow a similar trend to Os and Re, being positively correlated with Ir (Fig. 2c and d). In the same way, Ru and Rh concentrations in pyrrhotite and pentlandite from the semi-massive ore are the highest, ranging from ~18 to 260 ppb for Ru (with no preference for one of the two BMS), and from 28 to 199 ppb Rh in pyrrhotite and from 30 to 150 ppb Rh in pentlandite. These values decrease in the disseminated ore (usually below 40 ppb for Rh and below the detection limit for Ru, ~12–17 ppb) and more drastically in the chalcopyrite veinlet (below the detection limit, ~12–14 ppb)

Table 3
Laser ablation ICP-MS results for pyrrhotite, pentlandite, chalcopyrite and pyrite from the Aguablanca deposit.

Ore-type	*n*		^{61}Ni	^{59}Co	^{185}Re	^{189}Os	^{193}Ir	^{101}Ru[a]	^{103}Rh[a]	^{195}Pt	^{105}Pd[b]	^{197}Au	^{107}Ag	^{111}Cd	^{82}Se	^{209}Bi	^{125}Te	^{75}As
			wt.%	wt.%	ppm	ppb	ppb	ppb	ppb	ppb	ppb	ppb	ppm	ppm	ppm	ppm	ppm	ppm
Semi-massive ore																		
Pyrrhotite	38	Range	0.48–1.27	0.005–0.02	0.19–1.23	16–189	43–316	18–238	28–199	<10	<46	<6	0.09–1.83	0.01–0.34	55–80	0.16–3.88	0.4–2.6	<5
		AM	0.688	0.012	0.34	78	136	82	81				0.54	0.11	67	1.62	1.32	
		SD	0.131	0.006	0.18	49	77	62	50				0.38	0.07	5	1.1	0.56	
Pentlandite	27	Range	32.1–36.8	0.28–1.20	0.10–0.44	24–152	47–259	16–258	30–150	<10	466–5218	<7–35	0.36–7.73	0.01–0.50	45–63	0.18–14.65	0.1–2.6	<5
		AM	33.73	0.775	0.24	56	103	122	65		2212	10	2.74	0.15	55	3.08	1.03	
		SD	1.16	0.246	0.12	33	64	71	35		1292	9	1.78	0.13	4	3.94	0.57	
Pentlandite — flames	3	Range	32–34.2	0.12–0.70	0.15–0.27	33–125	61–244	67–152	16–137	<7	43–149	<6	2.1–10.3	0.04–0.13	36–51	0.31–9.63	0.9–2.2	<5
		AM	32.68	0.416	0.22	66	124	106	66		64		5.30	0.07	45	3.31	1.01	
		SD	0.98	0.292	0.06	51	104	43	63		58		4.43	0.05	8	5.17	0.7	
Chalcopyrite	8	Range	0.01–0.02	<0.001	<0.01–0.50	<6–87	<3–13			<8	<17–82	<4–20	7.9–22.8	3.1–5.8	43–71	1.18–9.11	0.9–3.2	<5
		AM	0.012		0.17						45	9	15.90	4.72	60	4.75	1.64	
		SD	0.004		0.19						28	7	5.15	0.89	9	2.72	0.79	
Idiomorphic pyrite	4	Range	0.05–0.15	0.59–0.99	0.04–0.19	27–298	98–622	46–719	4206–30,570	31–15,030	<46	<5	0.01–49		12–120	0.001–0.89	0.1–0.2	42–208
		AM	0.079	0.75	0.10	188	388	476	n.d.	n.d.			n.d.		n.d.	n.d.	0.17	n.d.
		SD	0.048	0.18	0.07	131	233	300									0.17	
Ribbon-like pyrite	8	Range	1.19–7.67	0.20–0.58	0.19–0.46	45–219	84–358	32–225	62–220	<10	<40	16–418	2.0–17		85–110	0.67–51.7	1.7–17	<2
		AM	3.46	0.42	0.34	105	191	119	115			163	10.30		99	17.42	5.19	
		SD	2.31	0.11	0.1	67	114	81	60			152	5.40		9	21.47	5.1	
Disseminated ore																		
Pyrrhotite	16	Range	0.54–0.82	0.005–0.023	0.01–0.44	<5–40	<4–45	<11–81	<9–76	<6	<41	<4	0.07–1.76	0.02–0.16	87–185	0.45–6.86	0.1–2.5	<5
		AM	0.667	0.014	0.12	16	13	22	22				0.27	0.08	136	2.72	0.68	
		SD	0.081	0.006	0.13	12	14	18	17				0.42	0.04	31	2.23	0.55	
Pentlandite	13	Range	30.6–36.6	0.80–1.36	<0.01–0.14	<5–36	<4–22	<6–71	<8–129	<7	539–7087	<3–266	0.52–8.98	0.01–1.91	64–165	0.06–7.98	0.7–13.9	<5
		AM	33.98	1.066	0.06	11	9	24	29		2771	36	1.82	0.32	102	2.71	3.15	
		SD	1.75	0.198	0.05	8	6	20	33		2253	72	2.26	0.57	24	2.34	3.55	
Chalcopyrite	15	Range	0.01–0.04	<0.001	<0.01	<10	<5			<5	68–407	10–170	12.1–47.2	7.3–30.6	83–117	0.80–8.35	0.7–5.0	<5
		AM	0.014								170	45	30.30	17.25	100	4.49	2.60	
		SD	0.01								99	48	10.60	8.33	12	1.92	1.24	
Chalcopyrite veinlet																		
Pyrrhotite	3	Range	0.78–0.99	0.02–0.04	<0.005	<7	<3	<15	<13	<7	<39	<4	0.22–1.15	0.08–0.23	55–59	0.81–1.36	0.5–1.1	<5
		AM	0.8	0.028									0.66	0.14	57	1.08	0.91	
		SD	0.178	0.010									0.47	0.08	2	0.28	0.34	
Pentlandite	3	Range	33.9–34.7	1.05–1.16	<0.003	<6	<4	<14	<12	<5	3592–6770	<4–84	1.0–1.3	0.2–2.7	43–49	1.11–4.36	0.6–2.7	<5
		AM	34.4	1.117							5053	33	1.22	1.08	46	2.36	1.53	
		SD	0.41	0.058							1604	45	0.18	1.44	3	1.75	1.1	
Chalcopyrite	7	Range	0.01–0.02	<0.001	<0.01	<7	<3			<5	30–191	<5–99	5.7–34.8	5.8–13.3	50–63	0.88–5.59	0.6–2.0	<5
		AM	0.012								83	35	15.01	8.99	57	2.43	1.04	
		SD	0.007								33	34	11.39	2.45	5	1.65	0.49	

n: number of grains analyzed; AM: arithmetic mean of n values; SD: standard deviation around arithmetic mean; < below the detection limit; n.d.: arithmetic mean not determined due to large variations in the values.
[a] Ru and Rh in chalcopyrite not reported due to interferences.
[b] In chalcopyrite, ^{108}Pd was used instead of ^{105}Pd to avoid ^{40}Ar^{65}Cu interference. ^{108}Pd was corrected for ^{108}Cd.

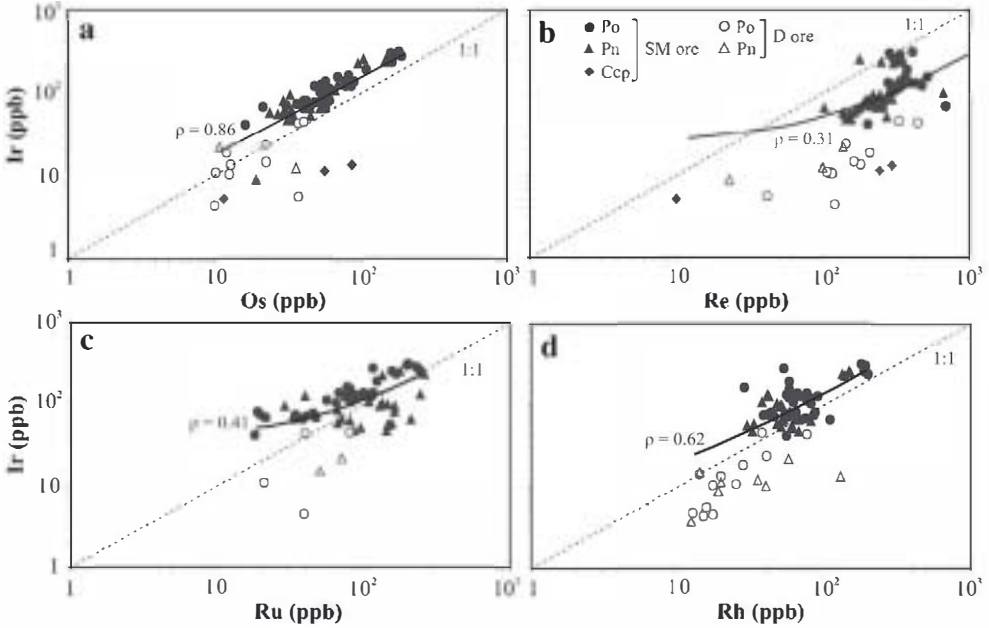

Fig. 2. Iridium versus a) Os, b) Re, c) Ru, and d) Rh contents in pyrrhotite, pentlandite and chalcopyrite from different ore types. Values below the detection limit were not plotted, hence no analyses for chalcopyrite from disseminated ore and BMS from chalcopyrite veins were represented. Linear regressions (solid lines), correlation coefficients (ρ) and 1:1 reference line (dashed lines) were represented for clarification.

(Fig. 3a and b). Ruthenium and Rh contents in the pentlandite flames are similar to those of the granular pentlandites (Table 3).

Palladium is the most abundant PGE detected within BMS. It occurs preferentially in pentlandite (466–7087 ppb), representing typically more than 80% of the total PGE found within this phase. Appreciable amounts of Pd in pentlandite have also been reported in other Ni–Cu–PGE sulfide deposits (e.g., Merensky Reef, Bushveld Complex, Godel et al., 2007, J-M Reef, Stillwater Complex, Godel and Barnes, 2008; Platreef, Bushveld Complex, Holwell and McDonald, 2007; and Creighton Mine, Sudbury, Dare et al. 2010a). Unlike Re, IPGE and Rh, Pd is relatively enriched in pentlandite from the disseminated and chalcopyrite-veined ores (from 539 to 7087 ppb, mean 2771, and from 3592 to 6770 ppb, mean 5053, respectively) relative to the semi-massive ore (from 466 to 5218 ppb, mean 2212) (Fig. 3b). More than 95% of PGE found in pentlandite from the disseminated and chalcopyrite-veined ores correspond to Pd. The Pd content in pentlandite also depends on the presence of chalcopyrite. Pentlandite grains in contact with chalcopyrite commonly have more Pd than those with no such contacts (Fig. 4). This is especially evident in intergranular pyrrhotite–pentlandite–chalcopyrite aggregates from the disseminated ore where pentlandite contains higher Pd values than those pentlandite grains located in chalcopyrite-free aggregates. In contrast to IPGE and Rh, whose abundances are similar in co-existing granular and flame-textured pentlandite, Pd is strongly depleted in flames (Table 3), containing ~95% less Pd than granular pentlandite. Palladium in pyrrhotite is invariably below detection limit (~39–46 ppb) in all ore-types. It is significantly more abundant in chalcopyrite from the disseminated ore (from 68 to 407 ppb) than in chalcopyrite from the semi-massive one (up to 82 ppb) (Fig. 3c). In the chalcopyrite veinlet, Pd in chalcopyrite varies between 30 and 191 ppb. Platinum is below the detection limit (~6–10 ppb) in all of the analyzed grains. During the laser ablation, several Pd–Pt–Bi–Te microinclusions were identified, mainly within pyrrhotite and pentlandite, by the presence of narrow and well-developed peaks

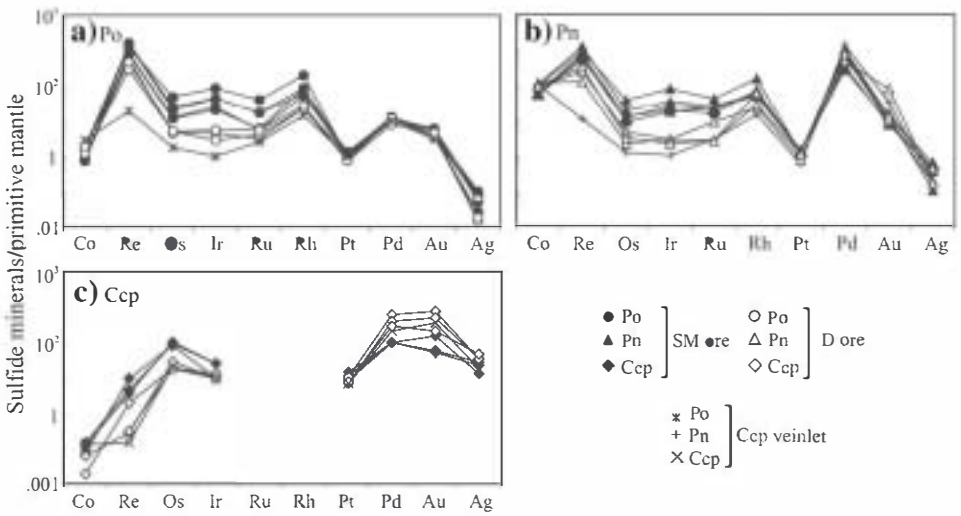

Fig. 3. Primitive mantle normalized metal patterns for pyrrhotite (a), pentlandite (b), and chalcopyrite (c). Points represent the average metal content normalized to primitive mantle values from McDonough and Sun (1995) in the sulfides of each sample. When data are below the detection limit, these values were employed.

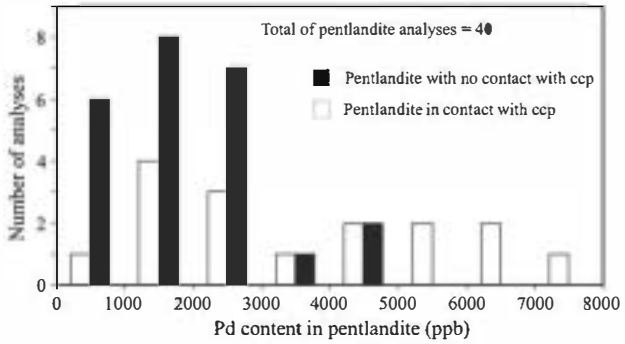

Fig. 4. Variation in the Pd content (ppb) between pentlandite in contact with chalcopyrite and pentlandite without any textural relationship with chalcopyrite.

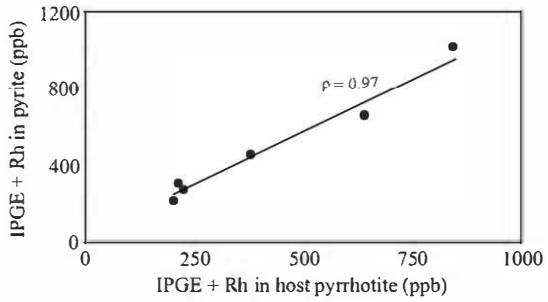

Fig. 6. Binary diagram showing the correlation between the IPGE and Rh contents for ribbon-like pyrites and their hosted pyrrhotites from semi-massive ore samples. Each point represents the analysis of a ribbon-like pyrite and its host pyrrhotite. Note the excellent positive correlation suggesting that pyrite inherits the PGE contents from pyrrhotite.

for these elements in the ICP-MS signal (Fig. 5a). The composition of these inclusions is consistent with the PGE mineralogy identified previously by Ortega et al. (2004), Piña et al. (2008) and Suárez et al. (2010).

Cobalt in the Aguablanca pentlandite ranges from 0.28 to 1.36 wt.%. Interestingly, Co concentrations in flame-textured pentlandite are lower than in granular pentlandite (Table 3). For the three ore types, Co in pyrrhotite varies from 50 to 200 ppm, and in chalcopyrite is generally <3 ppm. Cobalt shows good positive correlation with Ni ($\rho = 0.88$, not shown) and its correlation with Pd is only relatively good in pentlandite from semi-massive ore samples ($\rho = 0.48$, not shown).

Selenium is approximately evenly distributed between pyrrhotite, pentlandite and chalcopyrite in each sample, and is slightly more abundant in the disseminated ore (64–185 ppm) than in the semi-massive (36–80 ppm) and chalcopyrite-veined (43–63 ppm) ores. Bismuth preferentially occurs in chalcopyrite with similar concentrations for the three ore types (0.80–9.11 ppm). In pyrrhotite and pentlandite, Bi contents are usually lower (0.16–6.86 ppm and 0.06–14.65 ppm, respectively). The highest Te abundances have been found in pentlandite and chalcopyrite from the disseminated ore (0.7–13.9 ppm in pentlandite and 0.7–5.0 ppm in chalcopyrite). Arsenic concentrations are invariably below the detection limit (~5 ppm).

Chalcopyrite contains the majority of Ag (6–47 ppm) and Cd (3–31 ppm) found in BMS. These elements are positively correlated with each other. Silver contents are higher in chalcopyrite from the disseminated ore (12–47 ppm) than in that from the semi-massive one (8–23 ppm). Pentlandite has lower contents (0.4–9 ppm Ag, and 0.01–2.75 ppm Cd) than chalcopyrite, and most pyrrhotite contains less than 1 ppm Ag and 0.2 ppm Cd.

Gold is preferentially contained in chalcopyrite from the disseminated and chalcopyrite-veined ores (Fig. 3c), with values ranging between 10 and 170 ppb. Chalcopyrite in semi-massive ore samples has Au values close to the detection limit (~4–6 ppb) (Fig. 3c). In pentlandite, Au values are approximately equal for the three ore-types (from below the detection limit to 84 ppb, with the exception of one grain containing up to 266 ppb). Gold concentrations in pyrrhotite are below the detection limit.

4.2. Pyrite

There are notable differences in the concentrations of PGE among the large-grained idiomorphic pyrite and ribbon-like pyrite (Table 3). The idiomorphic pyrite, with most values ranging from 31 to 79 ppb, is the only BMS hosting Pt. One idiomorphic grain contains an unusually high Pt concentration, 15,030 ppb, which does not correspond to any microinclusion and does not correlate with any other element (Fig. 5b). In the idiomorphic pyrites, the concentrations of Rh (4.2–30.6 ppm), Co (0.59–0.99 wt.%) and As (42–208 ppm) are high and Ni is low (0.05–0.15 wt.%). There is no apparent correlation between these elements. In contrast, ribbon-like pyrite has low Pt (below the detection limit, ~10 ppb), Rh (62–220 ppb), Co (0.20–0.58 wt.%) and As (close to the detection limit, ~2 ppm), but high concentrations of Ni (1.19–7.67 wt.%), Au (16–418 ppb), Ag (2–17 ppm), Te (2–17 ppm), Bi (up to 51 ppm) and Re (0.19–0.46 ppm) relative to idiomorphic pyrite. Selenium is usually higher in the ribbon-like pyrite (85–110 ppm) than in idiomorphic pyrite (commonly less than 25 ppm). Osmium, Ir and Ru concentrations are slightly higher in idiomorphic pyrite than in ribbon-like pyrite (Table 3). There are good positive correlations between Os–Ir–Ru–Re, mainly in ribbon-like pyrite. Similarly, the concentrations of IPGE and Rh in ribbon-like pyrite grains are positively correlated with the concentrations of these elements in the host pyrrhotite (Fig. 6).

4.3. Mass balance calculations

In order to determine whether BMS are the principal carriers of PGE, we have calculated the percentage of each element present in solid solution in each BMS following the method described by Barnes et al. (2008). This calculation requires the contents of the elements in

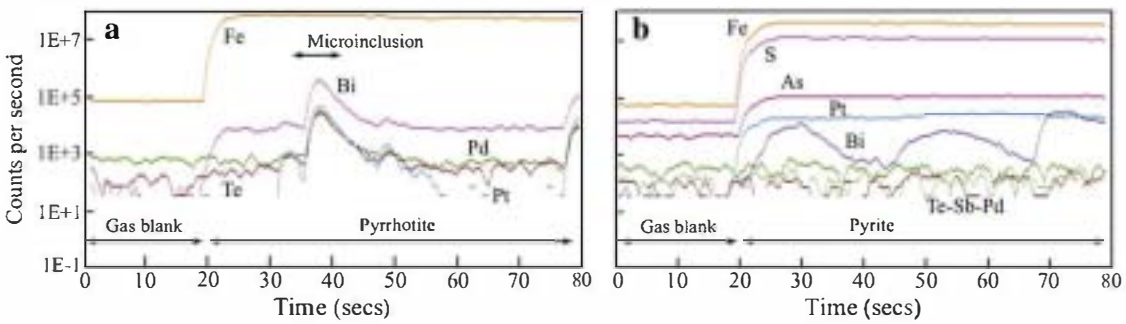

Fig. 5. Spectra of element abundances in pyrrhotite (a) and idiomorphic pyrite (b) from semi-massive ore samples obtained by LA-ICP-MS. The co-incident peaks of Bi, Te, Pd and Pt in pyrrhotite are interpreted as a microinclusion of Pd–Pt bismuthotelluride. By contrast, the Pt content in pyrite does not correspond to any microinclusions.

Table 4
Summary of whole rock concentrations (from Piña et al., 2008) of the samples used for LA-ICP-MS. Weight fractions of BMS are also indicated.

Sample	S	Ni	Cu	Co	Os	Ir	Ru	Rh	Pt	Pd	Au	Ag	Se	Bi	Te	As	Po	Pn	Ccp	Py
	wt.%	wt.%	wt.%	ppm	ppb	ppb	ppb	ppb	ppb	ppb	ppb	ppm	ppm	ppm	ppm	ppm	Weight fraction			
Semi-massive ore																				
Leo	20.12	5.85	0.62	1861	34	96	68	113	1187	1771	107	1.7	64	2.5	3.7	5	0.32	0.16	0.02	0.02
6715-416	26.24	6.41	0.22	1101	25	61	31	93	30	1193	20	2.1	57	11.17	2.1	2	0.42	0.18	0.01	0.06
6580-281	30.42	5.70	1.83	1790	75	219	121	263	467	676	56	2.1	65	3.77	1.1	6	0.51	0.16	0.05	0.04
6629-39	15.24	3.44	0.82	723	13	35	25	41	2244	768	39	2.5	36	4.57	2	5	0.20	0.10	0.02	0.06
6715-415	26.28	6.30	0.49	1225	21	57	26	98	84	907	49	2.6	64	10.64	2.4	6	0.44	0.18	0.01	0.03
Disseminated ore																				
6749-390	3.17	0.41	1.48	138	<2	<2	6	4	346	216	264	6.4	12	5.49	1.8	2	0.03	0.01	0.04	n.p.
AGU-5-29.7	3.76	0.80	0.85	212	<2	2	8	5	469	371	341	3.6	14	5.89	1.9	4	0.05	0.02	0.02	n.p.
6758-548.25	3.56	0.43	1.13	181	<2	<2	4	4	276	128	167	3.1	12	4.18	1.6	3	0.05	0.01	0.03	n.p.
Chalcopyrite veinlet																				
6479-45.6	7.07	0.97	4.76	284	3	8	8	12	737	618	833	9.9	19	3.26	1.3	5	0.03	0.03	0.14	n.p.

<2: below the detection limit (2 ppb). n.p.: not present.

whole rock (taken from Table 1 in Piña et al., 2008 and summarized in Table 4), the weight fraction of each BMS in the sample (Table 4; estimated as explained below using the bulk Ni, Cu and S concentrations and the mean content of Ni, Cu and S in each BMS) and the results of the in situ element analyses of the BMS (Table 3). For the weight fraction calculation, we have considered that all Cu in the whole rock is hosted by chalcopyrite, and Ni is hosted by pentlandite after extracting the concentration of Ni in olivine and pyroxene (~1000 ppm, average value, Piña et al., 2006). So, the weight fraction of chalcopyrite (F_{Ccp}) is given by Cu_{WR}/Cu_{Ccp}, where Cu_{WR} and Cu_{Ccp} represent the content of Cu in whole rock and chalcopyrite, respectively. The weight fraction of pentlandite (F_{Pn}) is given by

Table 5
Proportion (%) of each element hosted in pyrrhotite, pentlandite, chalcopyrite and sum BMS from the Aguablanca deposit.

Sample		Ni	Co	Os	Ir	Ru	Rh	Pt	Pd	Au	Ag	Se	Bi	Te
Semi-massive ore														
Leo	Po	3.8	3.0	65.0	45.2	40.1	15.0	*0.2*	*0.8*	*1.7*	11.6	34.7	5.8	14.0
	Pn	95.1	95.9	29.4	18.9	30.0	6.6	*0.1*	26.3	1.4	25.2	14.8	7.9	4.0
	Ccp	0.01	0.8	1.5	0.1			*0.02*	0.04	*0.1*	18.5	1.9	1.4	1.0
	Total BMS	99.0	99.7	95.9	64.2	70.1	21.6	0.3	27.1	3.2	55.3	51.4	15.1	19.0
6715-416	Po	4.0	3.0	67.1	45.8	38.4	35.8	*8.7*	*1.7*	*11.4*	7.7	46.0	10.8	15.8
	Pn	99.8	88.3	30.2	17.8	46.0	12.2	*4.8*	21.5	6.4	26.6	17.4	4.9	8.7
	Ccp													
	Total BMS	103.8	91.3	97.3	63.6	84.4	48.0	13.5	23.2	17.8	34.3	63.4	15.7	24.5
6580-281	Po	6.2	4.4	114.8	65.4	84.1	36.8	*0.7*	*3.3*	*3.1*	5.2	48.0	10.6	53.7
	Pn	95.9	87.9	26.9	17.8	27.4	8.6	*0.2*	90.0	3.7	6.2	12.7	8.9	9.6
	Ccp	0.0	1.3	2.4	0.2			*0.1*	0.3	1.6	26.7	4.3	7.7	6.8
	Total BMS	102.1	93.6	144.1	83.4	111.5	45.4	1.0	93.6	8.4	38.1	65.0	27.2	70.1
6629-39	Po	4.0	2.2	102.7	69.4	69.9	36.3	*0.1*	*1.3*	*2.5*	6.2	38.4	8.2	16.4
	Pn	92.2	85.2	30.1	22.1	40.5	13.6	*0.04*	28.6	3.3	16.5	14.6	12.8	6.8
	Ccp	0.0	1.5	5.7	0.6			*0.01*	0.1	0.4	20.7	4.1	4.1	1.6
	Total BMS	96.2	88.9	138.5	92.1	110.4	49.9	0.2	30.0	6.2	43.4	57.1	25.1	24.8
6715-415	Po	5.1	3.4	92.3	59.3	44.9	21.7	*3.7*	*2.2*	*3.7*	9.9	47.6	11.2	21.1
	Pn	92.7	86.5	25.7	17.3	78.7	7.7	*1.7*	20.8	3.1	17.8	15.2	5.8	8.6
	Ccp													
	Total BMS	97.8	89.9	118.0	76.6	123.6	29.4	5.4	23.0	6.8	27.7	62.8	17.0	29.7
Disseminated ore														
6749-390	Po	0.7	1.7	23.4	22.1	*8.2*	15.5	*0.07*	*0.7*	*0.1*	0.1	46.6	0.7	0.8
	Pn	80.7	76.6	5.4	3.6	*2.3*	13.5	*0.02*	15.0	0.1	0.6	10.9	0.7	4.2
	Ccp	0.1	0.1	*19.8*	*6.5*			*0.09*	4.9	1.3	18.1	38.7	4.1	7.6
	Total BMS	81.5	78.4	48.6	32.2	10.5	29.0	0.2	20.6	1.4	18.8	96.2	5.5	12.6
AGU-5-29.7	Po	0.6	3.2	42.3	23.7	13.1	22.1	*0.06*	*0.6*	*0.1*	0.8	49.7	4.8	1.5
	Pn	95.4	93.1	17.0	10.0	*3.4*	10.8	*0.03*	20.8	0.1	0.8	15.9	0.9	1.3
	Ccp	0.2	0.1	*7.3*	*5.0*			*0.03*	1.0	0.4	18.3	14.8	1.6	1.4
	Total BMS	96.2	96.4	66.6	38.7	16.5	32.9	0.1	22.4	0.5	19.9	80.4	7.3	4.2
6758-548.25	Po	0.7	5.4	41.8	42.9	34.6	31.6	*0.09*	*1.2*	*0.1*	0.2	45.8	1.4	2.9
	Pn	87.2	76.7	3.9	5.0	11.7	5.4	*0.02*	15.3	0.5	0.5	8.1	0.7	1.8
	Ccp	0.1	0.1	*10.0*	*5.1*			*0.07*	2.9	0.4	41.8	28.1	3.6	6.4
	Total BMS	88.0	82.2	55.7	53.0	46.3	37.0	0.2	19.4	1.1	42.5	82.0	5.7	11.1
Chalcopyrite veinlet														
6479-45.6	Po	2.4	2.9	*6.2*	*1.1*	*4.2*	*3.0*	*0.03*	*0.2*	*0.01*	0.2	8.8	0.1	2.1
	Pn	94.5	104.7	*3.3*	*1.1*	*4.7*	*2.6*	*0.02*	21.8	0.1	0.3	6.4	1.9	3.1
	Ccp	0.2	0.1	*31.1*	*4.8*			*0.1*	1.9	0.6	21.1	41.8	1.0	11.1
	Total BMS	97.0	107.7	40.6	7.0	8.9	5.6	0.1	23.9	0.7	21.6	57.0	3.0	16.3

Values in italics were obtained from laser results below the detection limit, hence they represent a maximum proportion.

$[Ni_{WR} - (X_{ol}Ni_{ol} + X_{px}Ni_{px})]/Ni_{Pn}$, where Ni_{WR}, Ni_{ol}, Ni_{px} and Ni_{Pn} are the Ni concentrations in whole rock, olivine, pyroxene and pentlandite, respectively, and X_{ol} and X_{px} represent the fractions of olivine and pyroxene in the rock, respectively. Finally, the weight fraction of pyrrhotite (F_{Po}) was determined assuming that the remaining S, after subtracting the S required by pentlandite and chalcopyrite, corresponds to pyrrhotite. Hence, F_{Po} is $(S_{WR} - F_{Pn}S_{Pn} - F_{Ccp}S_{Ccp})/S_{Po}$, where S_{WR} is the sulfur content in whole rock, and S_{Pn}, S_{Ccp} and S_{Po} are the average sulfur content in pentlandite, chalcopyrite and pyrrhotite, respectively. This calculation for the weight fraction of pyrrhotite is valid as long as no other BMS are present. In the disseminated and chalcopyrite-veined ore samples, this assumption is thus valid, but in semi-massive ore samples the presence of pyrite (up to 10 vol.%) must be taken into account. In these samples, the weight fraction of pyrrhotite has been obtained after determining optically the relative modal abundance of pyrrhotite and pyrite and then subtracting the S consumed by pyrite. The S consumed by pyrite was used for the calculation of the weight fraction of pyrite (F_{Py}) expressed as $(S_{WR} - S_{po+ccp+pn})/S_{Py}$, where $S_{po+ccp+pn}$ is the sulfur consumed by pyrrhotite, pentlandite and chalcopyrite, and S_{Py} is the average sulfur content in pyrite. Pyrite was not included in the mass balance calculations due to a number of reasons. Firstly, the relative modal proportion between idiomorphic pyrite and ribbon-like pyrite is variable even within individual samples. Furthermore, the PGE abundance ranges widely in a same textural type of pyrite, mostly in idiomorphic pyrites (Table 3). Finally, the number of analyses is not abundant enough to do representative calculations. Where whole rock concentrations were below the detection limit (i.e., Os and Ir in disseminated ore samples), these detection limit values were employed and the percentages obtained by the mass balance calculation represent minimum values. Similarly, we used the LA-ICP-MS detection limit values when in situ analyses were below the detection limit. In this case, these percentages represent maximum values. Results of the mass balance calculation are given in Table 5 and a histogram with the average percentages of each element hosted by BMS in the semi-massive and disseminated ores is shown in Fig. 7.

Pyrrhotite and, to a lesser extent, pentlandite account for a large proportion of Os, Ir, and Ru in the semi-massive ore samples (88%± 22 Os, 57%± 11 Ir, and 56%± 20 Ru for pyrrhotite; 28%± 2 Os, 19%± 2 Ir, and 45%± 20 Ru for pentlandite). In the disseminated ore, the amount of Os, Ir, and Ru present in pyrrhotite and pentlandite is much lower (36%± 11 Os, 30%± 11 Ir, and 19%± 14 Ru for pyrrhotite; 9%± 7 Os, 6%± 3 Ir, and 6%± 5 Ru for pentlandite). In these disseminated ore samples, the percentages of Os and Ir represent a minimum because the whole rock concentrations used correspond to the detection limit (2 ppb) and therefore these percentages are surely higher. The Os, Ir, and Ru weight fractions for pyrrhotite and pentlandite from the chalcopyrite veinlet are very low, considering that they represent a maximum value (10% Os, 2% Ir and 9% Ru in pyrrhotite plus pentlandite).

A moderate part of the Rh (22–50%) is within BMS in the semi-massive and disseminated ore samples. As for Os, Ir, and Ru, for a given sample, pyrrhotite hosts more Rh (15–37%) than pentlandite (5–14%). In the chalcopyrite veinlet, Rh in pyrrhotite and pentlandite is very low (<3% in both sulfides). Pentlandite accounts for 15–29% of whole-rock Pd. An exception to this is one semi-massive ore sample (6580-281) where 90% of the Pd is present within pentlandite. Chalcopyrite uniquely accounts for up to 5% of the Pd. As is common for other Ni–Cu–(PGE) sulfide ores (e.g., Kelly lake deposit, Sudbury, Huminicki et al., 2005; Merensky Reef, Bushveld Complex, Godel et al., 2007), Pt and Au are not present in any particular BMS with the exception of the traces of Pt (locally as high as 15 ppm) found within idiomorphic pyrite (Fig. 5b). The percentage of the whole rock Ag content that is hosted in the BMS ranges from 19 to 55%. In the semi-massive ore, pentlandite (19%± 8) and chalcopyrite (22%± 4) are the main BMS hosting Ag, whereas in the disseminated and chalcopyrite-veined ore samples, chalcopyrite is the only carrier of Ag (18–42%) because Ag percentages estimated for pyrrhotite and pentlandite are negligible (<1%). The Ag that is not present in BMS occurs as discrete phases such as argentopentlandite, identified within chalcopyrite (Piña et al., 2008) and commonly interpreted as an exsolution product (i.e., Gervilla et al., 1998; Szentpeteri et al., 2002). Most Co is hosted by pentlandite (77 to 96%), with pyrrhotite only accounting for 2 to 5%. In semi-massive ore samples, BMS account for 15 to 27% Bi and 19 to 30% Te (except for a sample where BMS account for 70% Te), whereas in disseminated and chalcopyrite-veined ore samples the amount of Bi and Te present in BMS is significantly lower (up to 7% Bi and 16% Te). Selenium is mostly within BMS (51–65% semi-massive ore; 80–96% in disseminated ore; and 57% in the chalcopyrite veinlet).

5. Discussion

On the basis of the BMS mineralogy and whole rock metal abundances, the different ore types of the Aguablanca Ni–Cu deposit have been interpreted to be the result of the fractionation and crystallization of an immiscible sulfide liquid (Ortega et al., 2004; Piña et al., 2008, 2010). The predominance of pyrrhotite in the semi-massive ore linked with the high pentlandite/chalcopyrite modal ratios (commonly above 4), low (Pd+Pt)/(IPGE+Rh) ratios (commonly between 1.7 and 10) and relatively high IPGE and Rh contents (Table 4) suggests that this ore represents a Fe-rich monosulfide solid solution (*mss*) cumulate. In contrast, the fractionated metal contents of the chalcopyrite veinlets with low IPGE and Rh abundances, and high Pd, Cu, and Au concentrations suggest that these likely formed from a Cu-rich sulfide liquid. BMS from the disseminated ore could represent either the crystallization of an original, unfractionated sulfide liquid or a fractionated sulfide liquid after *mss* crystallization (Piña et al., 2008). This interpretation is based on the relative abundance of Pt, Pd, and Au in comparison with the semi-massive ore, the low pentlandite/chalcopyrite modal ratios (0.06–0.31) and the high (Pd + Pt)/(IPGE + Rh) ratios (commonly higher than 34). We suggest that the hypothesis referring to a fractionated sulfide liquid is unlikely because the liquidus temperature of the silicate magma is significantly higher than that of a fractionated sulfide liquid, and thus

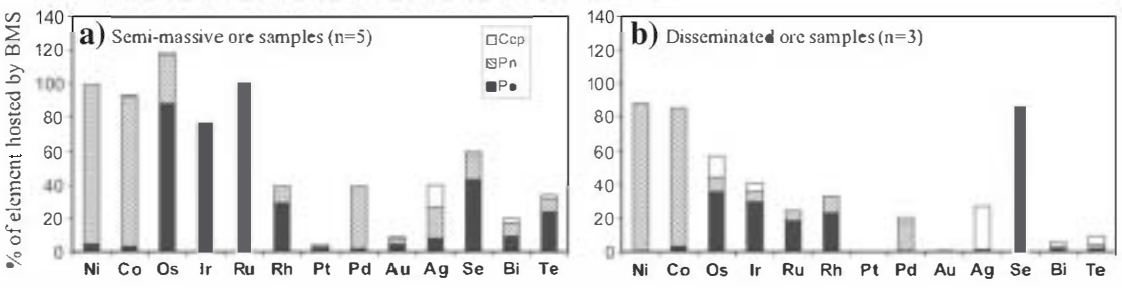

Fig. 7. Mass balance of the PGE and other chalcophile elements in base metal sulfides (BMS) from the semi-massive (a) and disseminated (b) ore, Aguablanca deposit, plotted as the proportion (%) of each element in pyrrhotite (Po), pentlandite (Pn), and chalcopyrite (Ccp).

it would be difficult for a fractionated sulfide liquid to disperse and form disseminated ore in partially solidified igneous rocks. Hence, the disseminated sulfides may represent an original sulfide liquid that crystallized in situ and was retained as droplets in the host gabbronorite. Furthermore, in many cases these droplets show separated Ni-rich and Cu-rich fractions (see Fig. 8B in Ortega et al., 2004), exemplifying that sulfide melt was retained and later underwent fractionation processes on a small scale.

Experimental work has demonstrated that PGE and chalcophile elements fractionate during the crystallization of *mss* from the sulfide melt (Fleet et al., 1993; Li et al., 1996; Barnes et al., 1997, 2001; Mungall, et al., 2005). Whereas Re, Os, Ir, Ru, Co, and Rh partition into the crystallizing *mss*, Pt, Pd, Cu, Au, Ag, Cd, and semi-metals (Bi, Te, Sb, and As) behave incompatibly and concentrate in the Cu-rich residual liquid. If fractionation of the sulfide liquid occurred at Aguablanca, then this mechanism could be the key to understanding the distribution of metals in the deposit. Fractionation would lead to concentration of Re, Os, Ir, Ru, and Co in the exsolution products of *mss* (pyrrhotite and pentlandite), whereas Pt, Pd, Au, Ag, and Cd would be concentrated in the crystallization products of the Cu-rich liquid, mainly chalcopyrite. However, other processes, such as crystallization of PGM and circulation of late magmatic and/or hydrothermal fluids, could modify the distribution of PGE in the ore. In the following sections, we will discuss the role played by these processes on the distribution of PGE in the Aguablanca Ni–Cu deposit.

5.1. Fractionation of the sulfide liquid

The LA-ICP-MS data obtained in this work indicate that the distribution of PGE in Aguablanca is largely controlled by their partitioning behavior during the fractionation of the parent sulfide liquid. Rhenium, Os, Ir, Ru, and minor Rh are accommodated in pyrrhotite and pentlandite from the semi-massive ore (i.e., *mss* cumulate) (Fig. 3a–b). Pentlandite typically exsolves from *mss* on cooling (Kelly and Vaughan, 1983), but Peregoedova and Ohnenstetter (2002) have shown that pentlandite can also originate via exsolution from heazlewoodite-*iss*. If this were the case, then the pentlandite should have lower Os, Ir, Ru and Rh contents than pyrrhotite, because *iss* does not concentrate any of these elements. However, in the semi-massive ore samples, Os, Ir, Ru and Rh are approximately equally distributed among coexisting pyrrhotite and pentlandite (Fig. 8), suggesting that this pentlandite exsolved from *mss*. In contrast, the pentlandite present in the chalcopyrite veinlet (i.e., Cu-rich sulfide liquid) contains very little IPGE and Rh (Table 3), so it could have exsolved from *iss* on cooling, or at least, from a fractionated sulfide liquid that was depleted in Re, IPGE and Rh by earlier crystallization of *mss*. Fig. 8 also shows that Os, Ir, and Rh are slightly preferentially concentrated in pyrrhotite, likely reflecting a preference of these elements for pyrrhotite against pentlandite during exsolution processes (e.g., Ballhaus and Sylvester, 2000; Holwell and McDonald, 2007). The apparent strong affinity of Rh for *mss* in Aguablanca points to relatively high S to metal ratios of the sulfide melt, because under these S-saturated or S-oversaturated conditions, Rh behaves as a compatible element during *mss* crystallization (Li et al., 1996; Mungall et al., 2005). Mass balance calculations indicate that pyrrhotite and pentlandite account for the majority of Os–Ir–Ru–Rh in the semi-massive ore samples (Table 5), in agreement with the almost total absence of IPGE-Rh-bearing discrete PGM in such ore. Mass balance calculations for Re have not been possible due to the lack of whole rock data. Nevertheless, Re is commonly hosted in BMS (Barnes et al., 2008) and since no Re-bearing phase has been found, most Re is inferred to be dominantly hosted within BMS. These observations imply that pyrrhotite and pentlandite retained most of the Os, Ir, Ru, and Rh budget of the *mss*. The interpretation that the pyrrhotite and pentlandite, enriched in IPGE and Rh, have been exsolved from *mss* and preserve its original concentrations has also been proposed for the Platreef of the Bushveld Complex (Holwell and McDonald, 2007) and for the massive ore of the Noril'sk deposit (Barnes et al., 2008).

Palladium has a different distribution to the IPGE and Rh in the Aguablanca ore. Mass balance calculations indicate that most Pd occurs as PGM, but a significant proportion (from 15 to 29%) also is in solid solution within pentlandite. A number of studies have shown that pentlandite is a fairly common Pd carrier in Ni–Cu–PGE deposits (i.e., Medvezky Creek Mine, Noril'sk, and Merensky Reef, Bushveld Complex, Barnes et al., 2008; J-M Reef, Stillwater Complex, Godel and Barnes, 2008; Platreef, Bushveld Complex, Holwell and McDonald, 2007 and Hutchinson and McDonald, 2008; Creighton deposit, Sudbury, Dare et al., 2010a). Pentlandite commonly exsolves from *mss* on cooling (Naldrett, 1969; Craig, 1973) and as Pd is relatively incompatible with *mss* ($D_{Pd}^{mss/sulf} = 0.005–0.44$, Fleet et al., 1993; Li et al., 1996; Mungall et al., 2005), one might expect that pentlandite

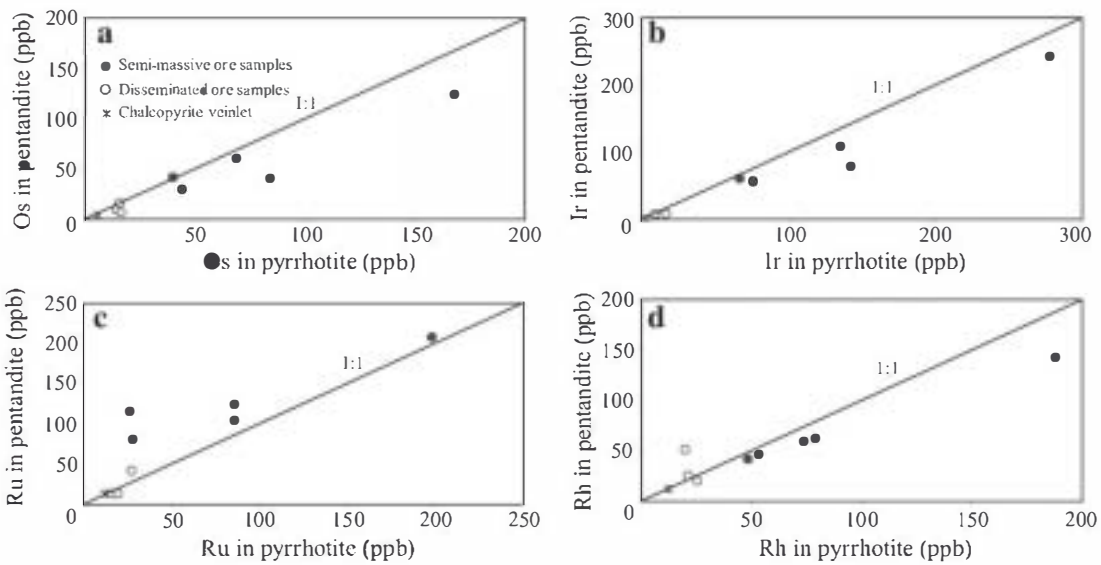

Fig. 8. Variation diagrams of the average content in Os (a), Ir (b), Ru (c), and Rh (d) among pyrrhotite and pentlandite that coexist in a same sample. When individual analyses were below the detection limit, these values were employed for the calculation of the mean value. Lines 1:1 indicate equal distribution of the PGE among pyrrhotite and pentlandite.

exsolved from *mss* contains very little Pd. However, some studies have suggested that some Pd does can enter *mss* and later concentrate in pentlandite during its exsolution in the same manner as the Co and Ni that were originally dissolved in *mss* eventually partitioned into pentlandite (Helmy et al., 2007; Holwell and McDonald, 2007; Dare et al., 2010a,b; Barnes and Dare, 2010). We suspect that in Aguablanca some Pd may also enter in *mss* as suggested by the common occurrence of Pd-bearing PGMs (interpreted as exsolution products) within pyrrhotite from semi-massive ore samples.

Barnes et al. (2006) and Dare et al. (2010a) have attributed the high Pd concentrations in pentlandite from Noril'sk and Sudbury Ni–Cu deposits, respectively, to Pd diffusion into pentlandite from *iss* and *mss* during cooling. The evidence observed by these authors leading to this interpretation has been also found at Aguablanca, namely, the Pd that enters into solid solution in pentlandite is influenced by the timing of pentlandite exsolution and by textural relationships with chalcopyrite (i.e., whether pentlandite is or is not in contact with chalcopyrite). Experimental studies have shown that, at high temperatures, *mss* can dissolve appreciable amounts of Pd (up to 11 wt.% at 900 °C), but with decreasing temperature, the solubility of Pd decreases drastically (0.4 wt.% at 500 °C) and as a result Pd enters into the pentlandite structure (Makovicky et al., 1986). Similarly, Peregoedova (1998) experimentally demonstrated that Pd (and Pt and Au) is incompatible in *iss* at ~840 °C. Besides, Kelly and Vaughan (1983) demonstrated that pentlandite first exsolves from *mss* at ~600 °C as granular pentlandite, and later at ~300 °C it starts to exsolve as flames within pyrrhotite. According to Dare et al. (2010a)'s diffusion model, the Pd content initially dissolved in *mss*/pyrrhotite and *iss* would start to be rejected to granular pentlandite at high temperatures (<650 °C). As a consequence, pyrrhotite and *iss* would become depleted in Pd and later, at low temperatures (~300 °C), Pd would not be available to diffuse into flame-textured pentlandite. At Aguablanca, the laser ablation results are in agreement with this diffusion model. Firstly, the flames of pentlandite are much poorer in Pd (and Co) than co-existing granular pentlandites (Table 3), indicating that pyrrhotite rejected almost the totality of Pd when the flames started to exsolve. In addition, pentlandite grains in contact with chalcopyrite typically have higher Pd values than those grains with no contact with chalcopyrite (Fig. 4), suggesting that chalcopyrite provided an extra source of Pd.

The laser ablation data is insufficient to test the two possibilities considered for the origin of the disseminated ore: (1) that it represents the crystallization of an original sulfide melt, (2) that it represents a fractionated sulfide liquid. The low Re, IPGE and Rh contents of the pyrrhotite and pentlandite in comparison with the values observed in the semi-massive ore samples can be indicative of both origins. Similarly, the pentlandite from the disseminated ore is slightly enriched in incompatible elements such as Pd and Au relative to the pentlandite from the semi-massive ore (Fig. 3b), but this observation is not necessarily indicative of a fractionated sulfide liquid because, as it has been shown above, sulfides without any fractionation can also show this enrichment (Pd diffusion from *mss* and Cu-rich portion). Fig. 9 can shed some light on the origin of the disseminated ore. This figure shows a pattern of the metals in pyrrhotite, pentlandite, and chalcopyrite from the semi-massive ore normalized to the average of the whole rock composition of the disseminated ore. Osmium to Rh are enriched in pyrrhotite and pentlandite by a factor of 3 to 15 relative to the disseminated ore, and Pt and Au are depleted by factors of 0.1 and 0.01. These values are within the range for the partition coefficients into *mss* (Barnes and Lightfoot, 2005 and references therein), so these data are consistent with the hypothesis of the disseminated ore representing an original sulfide liquid from which *mss* crystallized.

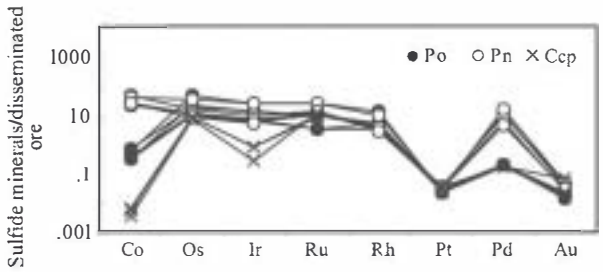

Fig. 9. Metal content in pyrrhotite, pentlandite and chalcopyrite from semi-massive ore samples normalized against the average whole rock content of the disseminated ore. When data are below the detection limit, these values were employed.

At Aguablanca, fractionation of *mss* resulted in only a minor amount of Cu-rich residual liquid, which concentrated incompatible elements such as Cu, Pd, Pt, Au, Ag, and Cd. Laser ablation data support the interpretation that chalcopyrite veinlets represent crystallization products of this Cu-rich liquid. Chalcopyrite in the chalcopyrite veinlet is slightly enriched in Cd and Au in comparison with chalcopyrite from semi-massive ore samples, and in addition, pyrrhotite and pentlandite have extremely low IPGE and Rh values (below the detection limit), and pentlandite hosts relatively high Pd and Au contents.

5.2. Crystallization of platinum-group minerals

Mass balance calculations indicate that a large proportion of Pd (~70%, the remainder held in pentlandite) and almost all Pt and Au are not present in any BMS (except for pyrite as discussed below). These elements must therefore occur as discrete PGM, and in fact, Pd and Pt have been found as bismuthotellurides (merenskyite, palladian mellonite, michenerite and moncheite) and arsenides (sperrylite) in the ore (Ortega et al., 2004; Piña et al., 2008; Suárez et al., 2010). Discrete gold-bearing phases are rare. Ortega et al. (2004) found two minute grains (possibly electrum) in pyrrhotite from semi-massive ore very close to a veinlet of chalcopyrite, and Suárez et al. (2010) identified eleven grains of native gold. To understand why both Pd and Pt are not present in BMS but as PGM, it is very useful to discuss the origin of the PGM.

Two different possibilities may be considered for the origin of the Pd–(Pt) bismuthotellurides in Aguablanca. These PGM could have formed by exsolution from the BMS during cooling or could have crystallized directly from an immiscible Te–Bi-rich liquid segregated from a fractionated sulfide melt (Holwell and McDonald, 2010). Experimental work by Helmy et al. (2007) demonstrated that a Te-rich (and othersemimetals such as Bi, Sb, As) melt can segregate from a fractionated sulfide melt as long as the Te concentration in this melt exceeds its solubility in Fe-rich *mss* and *iss*, ~0.2 wt.%. These authors also demonstrated that Pd and Pt are strongly complexed by this Te-rich melt. At Aguablanca, it is difficult to infer the immiscibility of a Te-rich melt because, if all the Te present in the mineralized samples were assigned to the BMS, then the sulfide liquid would only have ~15 ppm. This amount of Te can easily dissolve in the sulfide at high temperatures, and therefore Pd can stay available in the sulfide liquid to enter later in solid solution within BMS. Hence, we suggest that PGM formation by exsolution from pyrrhotite and pentlandite is a more plausible explanation. Makovicky et al. (1986) demonstrated that PGE initially dissolved at high temperature in *mss* can subsequently exsolve as PGM on cooling. At Aguablanca, Pd and Pt as well as Te, Bi, and As, initially in pyrrhotite and pentlandite, were no longer able to remain dissolved in the BMS upon cooling and were expelled giving rise to the observed PGM assemblage. In agreement with this, most Bi and Te (generally more than 75% according to the mass balance calculation, Table 5) occur as discrete grains and, indeed, Piña et al. (2008) not only identified Pd–Pt-bismuthotellurides but tsumoite (BiTe), tellurobismuthite (Bi_2Te_3), bismuthinite (Bi_2S_3) and tetradimite (Bi_2Te_2S) located invariably within the BMS. The presence of Pd-bismuthotellurides enclosed within pyrrhotite, pentlandite and chalcopyrite allows us to infer that Pd, Te and Bi were present in both

mss and *iss*, and that the exsolution process took place after pentlandite exsolution from *mss*. Several lines of evidence support an origin of the bismuthotellurides as exsolutions from the BMS: (a) Most of the PGM (76% of a total of 301 PGM, Piña et al., 2008) occur included in individual BMS. Platinum-group minerals crystallizing from an immiscible semimetal-rich melt would instead tend to occur around the margins of BMS and rarely enclosed in them (Tomkins, 2010). (b) The Pd–Pt bismuthotellurides exhibit textures (mostly <10 μm in size, rounded grains and laths, Fig. 6 of Piña et al., 2008) also observed in PGM produced in experiments where *mss* is slowly cooled (Peregoedova et al., 2004). (c) The merenskyite compositions at Aguablanca (characterized by high Bi replacing Te) reveal crystallization temperatures below 500 °C, and michenerite is stable only below this temperature (Hoffman and MacLean, 1976). This temperature is well below the solidus of a sulfide melt so these PGM were not able to crystallize directly from this melt. (d) The identification of tiny inclusions enriched in Pd–Pt–Bi–Te during laser ablation points to exsolution processes during cooling (e.g. Helmy et al., 2007).

In contrast to Pd and Pt, IPGE- and Rh-bearing phases are very scarce throughout the deposit. Ortega et al. (2004) has identified minor, tiny (<3 μm) grains containing Os–Ir–As–S, Ir–As–S and Ir–Pt–As. The first, probably a member of the irarsite–osarsite solid solution series, was found enclosed in chalcopyrite from the disseminated ore, and the Ir–As–S and Ir–Pt–As phases were identified in a single veinlet of chalcopyrite within chalcopyrite and pyrrhotite, respectively. None of these grains were found in semi-massive ore samples where BMS account for the majority of the Os, Ir, and Ru of the rock, but were identified in samples where the percentage of these elements in the BMS is significantly lower (Table 5). One would like to suggest that the amount of Os–Ir–(Ru, Rh) that is not present in the BMS from the disseminated and chalcopyrite-veined ores occurs as early-crystallized sulfarsenides. At some deposits, as for example in the Kylmakoski Ni–Cu deposit (Gervilla et al., 1998) and the Creighton deposit, Sudbury (Dare et al., 2010a,b), these As-rich PGM crystallize before *mss* crystallization and, as a consequence, the sulfide melt became impoverished in these elements. A similar hypothesis may be used for these samples in Aguablanca, but the PGM studies have not conclusively identified enough sulfarsenide grains to confirm this idea. In contrast, at Aguablanca the low As concentrations of the mineralized rocks (2–7 ppm, Table 1, Piña et al., 2008, 19–94 ppm normalized to 100% sulfide, lower than the As content which can dissolve into *mss* at 850 °C, ~0.2 wt.%, Makovicky et al., 1992) likely prevented the overall saturation in IPGE-bearing sulfarsenides, holding the IPGE and Rh in the sulfide melt. Furthermore, although it seems evident that pyrrhotite and pentlandite from the disseminated ore samples host less PGE than in the semi-massive ones, the percentages obtained from the mass balance calculation must be taken with caution because they represent a minimum value (the whole rock data used is the detection limit) and, surely, the real value is much higher.

5.3. Role of pyrite as carrier of PGE

Pyrite is not a common BMS carrier of PGE in Ni–Cu–PGE sulfide deposits. Until now, only a few studies have found traces of these elements in pyrite. For example, Oberthür et al. (1997) found pyrites with up to 233 ppm Pt and 40 ppm Ru in the Main Sulfide Zone from the Great Dyke in Zimbabwe. Gervilla and Kojonen (2002) also identified pyrite with traces of Pd close to 30 ppm in the Keivitsansarvi Ni–Cu–PGE deposit, Finland. Recently, Dare et al. (in press) described two main generations of pyrite with distinct PGE contents in the McCreedy East deposit of the Sudbury Igneous Complex: (1) early-formed idiomorphic PGE-enriched pyrites formed by exsolution from *mss* (113 ppm Rh, 1–6 ppm Os–Ir–Ru and 0.1 ppm Pt), and (2) PGE-poor pyrites formed from the alteration of *mss* by late magmatic/hydrothermal fluids (<0.09 ppm Rh, <0.01 ppm Os–Ir–Pt). Also recently, Djon et al. (2010) identified pyrites from the sulfide ores of the Lac-des-Iles Complex with 0.01–0.3 ppm Os–Ru, 0.008–0.06 ppm Ir, and up to 1 ppm Rh and Pt. All these results reveal that pyrite may be an unsuspected carrier of PGE in Ni–Cu–PGE ore deposits. In Aguablanca, the two main textural types of pyrite (i.e., large idiomorphic grains and ribbon-like aggregates) have very different PGE concentrations (Table 3), suggesting that they likely formed at different times and by different processes. Ribbon-like pyrite is characterized by having similar IPGE and Rh contents to those of its host pyrrhotite showing an excellent positive correlation (Fig. 6). This correlation suggests that ribbon-like pyrites likely inherited the IPGE and Rh concentrations of host pyrrhotite. Based on similar positive correlation, Dare et al. (in press) and Djon et al. (2010) have proposed this same interpretation for secondary pyrites from the McCreedy deposit of the Sudbury Igneous Complex and sulfide ores of the Lac-des-Iles Complex, respectively. Ortega et al. (2004) and Piña et al. (2008) have suggested that ribbon-like pyrite likely formed during the circulation of postmagmatic hydrothermal fluids, likely under higher fO_2 and fS_2 conditions than the sulfide assemblage. By contrast, the origin of idiomorphic pyrite is not well constrained. Contrarily to ribbon-like pyrite, idiomorphic pyrite hosts Pt with values as high as 15 ppm and high Rh contents (4.2–30.6 ppm). It is not clear if these Pt–Rh-rich pyrites are exsolution products from *mss* on cooling or alteration products of pyrrhotite like ribbon-like pyrites. In the McCreedy deposit of the Sudbury Igneous Complex, Dare et al. (in press) described IPGE-rich euhedral pyrites with the concentrations of these elements showing oscillatory zoning that was interpreted as having formed early at high temperature by exsolution from S-rich *mss*. In Aguablanca, the relatively high S to metal ratio interpreted from the compatible behavior of Rh in *mss* may have favored the exsolution of pyrite from a S-rich *mss*, but then it would be difficult to explain the enrichment of Pt in these grains because it is a strongly incompatible element in *mss*. Besides, the origin of Pt–Rh-rich pyrite in Aguablanca may be related to the hydrothermal remobilization of Pt from the PGM to the pyrite. Based on the marked Pt (and Au) negative anomalies in 100% sulfide, mantle-normalized metal abundance patterns and the erratic distribution of Pt throughout the deposit (even within individual ore-types), Piña et al. (2008) suggested that Pt (and Au) has likely undergone hydrothermal remobilization at small scale. Mineralogical evidence supporting this idea includes irregular edges of sperrylite at the contact with secondary chlorite suggesting partial dissolution of sperrylite by hydrothermal solutions (see Fig. 8c in Piña et al., 2008). Suárez et al. (2010) have also found in their study of the PGE mineralogy in the Aguablanca gossan that sperrylite can be eventually dispersed and corroded by post-magmatic hydrothermal fluids when alteration is especially intense. Therefore, post-magmatic hydrothermal fluids could partially remobilize Pt and later could be responsible for the replacement of pyrrhotite by pyrite. Pyrite has a sperrylite-like crystal structure and thus the positions occupied by Fe^{2+} can also be occupied by Pt^{2+}, so pyrite may be a favorable mineral to host significant amounts of Pt. Further work will be needed to well contrain the origin of pyrite and its role as a carrier of these elements in the deposit.

6. Conclusions

This LA-ICP-MS study has revealed the role played by the BMS as carriers of PGE and other chalcophile elements in the Aguablanca deposit. The majority of Re, Os, Ir, Ru and Rh occur within pyrrhotite and pentlandite, mainly in the semi-massive ore (i.e., *mss* cumulate) where these elements are preferentially concentrated. Most Pd (~70%) and almost all Pt occur as discrete PGM (Pd–Pt bismuthotellurides and Pt-arsenides). The rest of Pd is present in solid solution within pentlandite and a minor amount in chalcopyrite. Pentlandite is also the main carrier of Co and chalcopyrite hosts significant amounts of Ag and Cd. Gold is not found in BMS and likely occurs as electrum.

This distribution of the platinum-group and chalcophile elements is a result of the complex behavior of these elements during the magmatic and postmagmatic evolution of the Aguablanca ore. Platinum-group and chalcophile elements, originally collected by the sulfide melt, behaved differently during the sulfide fractionation in accordance with their partition coefficients between *mss* and Cu-rich sulfide liquid. Rhenium, Os, Ir, Ru and Rh were preferentially partitioned into *mss*. With cooling, *mss* changed to pyrrhotite and exsolved pentlandite, and these elements remained in solid solution within both phases but preferentially within pyrrhotite. The incompatible elements Pd, Pt, Au, Ag and Cd were concentrated into the Cu-rich sulfide liquid. This fractionated liquid formed minor chalcopyrite veinlets with BMS depleted in IPGE and Rh, and chalcopyrite hosting significant amounts of Ag, Pd, Cd, and Au. In spite of the incompatible behavior of Pd, pentlandite is the main BMS host of Pd, even in the semi-massive ore where pentlandite was exsolved from *mss*. The data suggest that the presence of Pd in pentlandite may be due to Pd diffusion into pentlandite from *mss* and chalcopyrite upon cooling. Our model also suggests that the PGM formed via exsolution from the BMS; during cooling, Pd and Pt, initially dissolved in pyrrhotite, pentlandite and chalcopyrite, were expelled along with Bi, Te and As, to form the observed PGM assemblage.

Finally, this study has revealed that pyrite can host appreciable amounts of PGE. The two main types of pyrite identified in Aguablanca ore (i.e., large idiomorphic grains and ribbon-like aggregates) contain distinct PGE concentrations indicating that they likely were formed at different times and by different processes. The idiomorphic pyrite is the only BMS hosting Pt and has relatively high Rh contents, whereas the ribbon-like pyrite does not contain Pt and hosts similar IPGE and Rh concentrations to those of the pyrrhotite. The ribbon-like pyrite seems to be secondary in origin and it likely inherited the PGE abundances of the host pyrrhotite that it replaced. By contrast, the origin of the idiomorphic pyrite is uncertain and further work will be necessary to better understand its genesis.

Supplementary materials related to this article can be found online at doi:10.1016/j.chemgeo.2011.02.010.

Acknowledgements

The authors are very grateful to Río Narcea Recursos S.A. for the facilities given for carrying on this research. We would like to thank Dany Savard for his assistance with the laser ablation analysis. Professor J. González de Tánago and Mr. A. Larios of the University Complutense of Madrid kindly assisted in the electron microprobe analyses. We greatly acknowledge Dr. Sarah Dare for her valuable suggestions and discussions which have improved the manuscript. We thank two reviewers Mr. Pedro Jugo and Andy Tompkins for their constructive reviews and Mr. James Brenan for his editorial input which have helped to improve the manuscript. This research was financed by the Spanish research project BTE2003-03599 and the Canada Research Chair in Magmatic Metallogeny.

References

Ballhaus, C., Sylvester, P., 2000. Noble metal enrichment processes in the Merensky Reef, Bushveld Complex. J. Petrol. 41, 545–561.

Barnes, S.-J., Dare, S.A.S., 2010. Pd diffusion into pentlandite evidence from laser ablation. Goldschmidt Conference Abstract 2010, p. A54.

Barnes, S.-J., Lightfoot, P.C., 2005. Formation of magmatic nickel sulfide deposits and processes affecting their copper and platinum group element contents. Econ. Geol. 100th Anniversary Volume, 179–213.

Barnes, S.-J., Makovicky, E., Karup-Moller, S., Makovicky, M., Rose-Hanson, J., 1997. Partition coefficients for Ni, Cu, Pd, Pt, Rh and Ir between monosulfide solid solution and sulfide liquid and the implications for the formation of compositionally zoned Ni–Cu sulfide bodies by fractional crystallization of sulfide liquid. Can. J. Earth Sci. 34, 366–374.

Barnes, S.-J., van Achterbergh, E., Makovicky, E., Li, C., 2001. Proton microprobe results for the partitioning of platinum-group elements between monosulphide solid solution and sulphide liquid. S. African J. Geol. 104, 275–286.

Barnes, S.-J., Cox, R.A., Zientek, M.L., 2006. Platinum-group element, Gold, Silver and Base Metal distribution in compositionally zoned sulfide droplets from the Medvezky Creek Mine, Noril'sk, Russia. Contrib. Mineral. Petrol. 152, 187–200.

Barnes, S.-J., Prichard, H.M., Cox, R.A., Fisher, P.C., Godel, B., 2008. The location of the chalcophile and siderophile elements in platinum-group element ore deposits (a textural, microbeam and whole rock geochemical study): implications for the formation of the deposits. Chem. Geol. 248, 295–317.

Cabri, L.J., Sylvestor, P.L., Tubrett, M.N., Peregoedova, A., Laflamme, J.H.G., 2003. Comparison of LAM-ICP-MS and micro-PIXE results for Palladium and Rhodium in selected samples of Noril'sk and Talnakh sulfides. Can. Mineral. 41, 321–329.

Carvalhosa, B.A., 1965. Contribuçao para o conhecimiento geologico da regiao entre Portel y Fichalo (Alentejo). Mem. Servicio Geol. Port. 11, 1–130.

Casquet, C., Galindo, C., Tornos, F., Velasco, F., Canales, A., 2001. The Aguablanca Cu–Ni ore deposit (Extremadura, Spain), a case of synorogenic orthomagmatic mineralization: age and isotope composition of magmas (Sr, Nd) and ore (S). Ore Geol. Rev. 18, 237–250.

Craig, J.R., 1973. Pentlandite–pyrrhotite and other low temperature relations in the Fe–Ni–S system. Am. J. Sci. 273, 496–510.

Crocket, J.H., Fleet, M.E., Stone, W.E., 1992. Experimental partitioning of osmium, iridium, and gold between basalt melt and sulfide liquid at 1300 °C. Austr J. Earth Sci. 39, 427–432.

Dare, S.A.S., Barnes, S.-J., Prichard, H.M., 2010a. The distribution of platinum-group elements (PGE) and other chalcophile elements among sulfides from Creighton Ni–Cu–PGE sulfide deposit, Sudbury, and the origin of palladium in pentlandite. Mineral. Deposita 45, 765–783.

Dare, S.A.S., Barnes, S.-J., Prichard, H.M., Fisher, P.C., 2010b. The timing and formation of platinum-group minerals from the Creighton Ni–Cu–platinum-group element sulfide deposit, Sudbury, Canada: early crystallization of PGE-rich sulfarsenides. Econ. Geol. 105, 1071–1096.

Dare, S.A.S., Barnes, S.-J., Prichard, H.M., Fisher, P.C., in press. Chalcophile and platinum-group element (PGE) concentrations in the sulfide minerals of the McCreedy East, Sudbury, Canada, and the origin of PGE in pyrite. Mineral. Deposit.

Djon, M.L.N., Barnes, S.-J., Gomwe, T.S., 2010. Contrasting Pd-bearing phases from the mineralized zones of the Lac-Des-Iles Complex (Ontario, Canada). Abstract, 11th International Platinum Symposium (Sudbury, Canada).

Fleet, M.E., Stone, W.E., Crocket, J.H., 1991. Partitioning of palladium, iridium, and platinum between sulfide liquid and basalt melt: effects of melt composition concentration and oxygen fugacity. Geochim. Cosmochim. Acta 55, 2545–2554.

Fleet, M.E., Chryssoulis, S.L., Stone, W.E., Weisener, C.G., 1993. Partitioning of platinum-group elements and Au in the Fe–Ni–Cu–S system: experiments on the fractional crystallization of sulfide melt. Contrib. Mineral. Petrol. 115, 36–44.

Gervilla, F., Kojonen, K., 2002. The platinum-group minerals in the upper section of the Keivitsansarvi Ni–Cu–PGE deposit, northern Finland. Can. Mineral. 40, 377–394.

Gervilla, F., Papunen, H., Kojonen, K., Johanson, B., 1998. Platinum-, palladium- and gold-rich arsenide ores from the Kylmäkoski Ni–Cu deposit (Vammala Nickel Belt, SW Finland). Min. Petrol. 64, 163–185.

Godel, B., Barnes, S.-J., 2008. Platinum-group elements in sulfide minerals and the whole rocks of the J-M Reef (Stillwater Complex): implication for the formation of the reef. Chem. Geol. 248, 272–294.

Godel, B., Barnes, S.-J., Maier, W.D., 2007. Platinum-group elements in sulphide minerals, platinum-group minerals, and whole-rocks of the Merensky Reef (Bushveld Complex, South Africa): implications for the formation of the Reef. J. Petrol. 48, 1569–1604.

Helmy, H.M., Ballhaus, C., Berndt, J., Bockrath, C., Wohlgemuth-Ueerwasser, C., 2007. Formation of Pt, Pd and Ni tellurides: experiments in sulphide–telluride systems. Contrib. Mineral. Petrol. 153, 577–591.

Hoffman, E., MacLean, W.H., 1976. Phase relations of michenerite and merenskyite in the Pd–Bi–Te system. Econ. Geol. 71, 1461–1468.

Holwell, D.A., McDonald, I., 2007. Distribution of platinum-group elements in the Platreef at Overysel, northern Bushveld Complex: a combined PGM and LA-ICP-MS study. Contrib. Mineral. Petrol. 154, 171–190.

Holwell, D.A., McDonald, I., 2010. A review of the behaviour of platinum group elements within natural magmatic sulfide ore systems: the importance of semimetals in governing partitioning behaviour. Platinum Met. Rev. 54, 26–36.

Huminicki, M.A.E., Sylvester, P.J., Cabri, L.J., Lesher, C.M., Tubrett, M., 2005. Quantitative mass balance of platinum group elements in the Kelly Lake Ni–Cu–PGE deposit, Copper Cliff Offset, Sudbury. Econ. Geol. 100, 1631–1646.

Hutchinson, D., McDonald, I., 2008. Laser ablation ICP-MS study of platinum-group elements in sulphides from the Platreef at Turfspruit, northern limb of the Bushveld Complex, South Africa. Mineral. Deposit. 43, 695–711.

Kelly, D.P., Vaughan, D.J., 1983. Pyrrhotine–pentlandite ore textures: a mechanistic approach. Miner. Mag. 47, 453–463.

Li, C., Barnes, S.-J., Makovicky, E., Rose-Hansen, J., Makovicky, M., 1996. Partitioning of Ni, Cu, Ir, Rh, Pt and Pd between monosulfide solid solution and sulfide liquid: effects of composition and temperature. Geochim. Cosmochim. Acta 60, 1231–1238.

Lunar, R., Romeo, I., Piña, R., Capote, R., Ortega, L., Gervilla, F., Quesada, C., Tejero, R., 2008. El yacimiento de Ni–Cu–(EGP) de Aguablanca (Macizo Ibérico): Marco tectónico, mineralogía, geoquímica, geocronología y modelo metalogenético. Instituto Geológico y Minero de España, Serie de Recursos Minerales, Madrid. 252 pp.

Makovicky, M., Makovicky, E., Rose-Hansen, J., 1986. Experimental studies on the solubility and distribution of platinum-group elements in base metal sulphides in platinum deposits. In: Gallagher, M.J., Ixer, R.A., Neary, C.R., Pritchard, H.M. (Eds.), Metallurgy of Basic and Ultrabasic Rocks. Institute of Mining and Metallurgy, London, pp. 415–425.

Makovicky, M., Makovicky, E., Rose-Hansen, J., 1992. The phase system Pt–Fe–As–S at 850 °C and 470 °C. Neuss. Jahrb. Mineral. 10, 441–453.

McDonough, W.F., Sun, S.-S., 1995. The composition of the Earth. Chem. Geol. 120, 223–253.

Mungall, J.E., Andrews, R., Cabri, L.J., Sylvester, P.J., Tubrett, M., 2005. Partitioning of Cu, Ni, An, and platinum-group elements between monosulfide solid solution and sulfide melt under controlled oxygen and sulfur fugacities. Geochim. Cosmochim. Acta 69, 4349–4360.

Naldrett, A.J., 1969. A portion of the Fe–S–O and its application to sulfide ore magmas. J. Petrol. 10, 171–201.

Oberthür, T., Cabri, L.J., Weiser, T.W., McMahon, G., Müller, P., 1997. Pt, Pd and other trace elements in sulfides of the main sulfide zone, Great Dyke, Zimbabwe: a reconnaissance study. Can. Mineral. 35, 597–609.

Ortega, L., Lunar, R., García-Palomero, F., Moreno, T., Martín Estévez, J.R., Prichard, H.M., Fisher, P.C., 2004. The Aguablanca Ni–Cu–PGE deposit, southwestern Iberia: magmatic ore-forming processes and retrograde evolution. Can. Mineral. 42, 325–335.

Peach, C.L., Mathez, E.A., Keays, R.R., 1990. Sulfide melt-silicate melt distribution coefficients for noble metals and other chalcophile elements as deduced from MORB: implications for partial melting. Geochim. Cosmochim. Acta 54, 3379–3389.

Peregoedova, A.V., 1998. The experimental study of the Pt–Pd-partitioning behaviour between monosulfide solid solution and Cu–Ni-sulfide melt at 900–840 °C. 8th International Platinum Symposium Abstracts: Geol Soc. South Africa and South African Institute of Mining and Metallurgy Symposium Series S18, pp. 325–327.

Peregoedova, A.V., Ohnenstetter, M., 2002. Collectors of Pt, Pd and Rh in a S-poor Fe–Ni–Cu-sulfide system at 760 °C: results of experiments and implications for natural systems. Chem. Geol. 208, 247–264.

Peregoedova, A.V., Barnes, S.-J., Baker, D.R., 2004. The formation of Pt–Ir alloys and Cu–Pd rich sulfide melts by partial desulfurization of Fe–Ni–Cu sulfides: results of experiments and implications for natural systems. Chem. Geol. 208, 247–264.

Piña, R., Lunar, R., Ortega, L., Gervilla, F., Alapieti, T., Martínez, C., 2006. Petrology and geochemistry of mafic–ultramafic fragments from the Aguablanca (SW Spain) Ni–Cu ore breccia: implications for the genesis of the deposit. Econ. Geol. 101, 865–881.

Piña, R., Gervilla, F., Ortega, L., Lunar, R., 2008. Mineralogy and geochemistry of platinum-group elements in the Aguablanca Ni–Cu deposit (SW Spain). Mineral. Petrol. 92, 259–282.

Piña, R., Romeo, I., Ortega, L., Lunar, R., Capote, R., Gervilla, F., Tejero, R., Quesada, C., 2010. Origin and emplacement of the Aguablanca magmatic Ni–Cu–(PGE) sulfide deposit, SW Iberia: a multidisciplinary research. Geol. Soc. Amer. Bull. 122, 915–925.

Quesada, C., 1991. Geological constraints on the Paleozoic tectonic evolution of tectonostratigraphic terranes in Iberian Massif. Tectonophysics 185, 225–245.

Romeo, I., Lunar, R., Capote, R., Quesada, C., Dunning, G.R., Piña, R., Ortega, L., 2006. U/Pb age constraints on Variscan Magmatism and Ni–Cu–PGE metallogeny in the Ossa-Morena zone (SW Iberia). J. Geol. Soc. London 163, 837–846.

Romeo, I., Tejero, R., Capote, R., Lunar, R., 2008. 3D gravity modelling of the Aguablanca Stock, tectonic control and emplacement of a Variscan gabbronorite bearing a Ni–Cu–PGE ore, SW Iberia. Geol. Mag. 145, 345–359.

Suárez, S., Prichard, H.M., Velasco, F., Fisher, P.C., McDonald, I., 2010. Alteration of platinum-group minerals and dispersion of platinum-group elements during progressive weathering of the Aguablanca Ni–Cu deposit, SW Spain. Mineral. Deposit. 45, 331–350.

Szentpeteri, K., Watkinson, D.H., Molnar, F., Jones, P.C., 2002. Platinum-group element deposits, Cooper Cliff North area, Sudbury, Canada. Econ. Geol. 97, 1459–1470.

Tomkins, A.G., 2010. Wetting facilitates late-stage segregation of Precious Metal-enriched sulfosalt melt in magmatic sulfide systems. Geology 38, 951–954.

Tornos, F., Casquet, C., Galindo, C., Velasco, F., Canales, A., 2001. A new style of Ni–Cu mineralization related to magmatic breccia pipes in a transpressional magmatic arc, Aguablanca, Spain. Mineral. Deposit. 36, 700–706.

Vegas, R., 1968. Sobre la existencia de Precámbrico en la Baja Extremadura. Estud. Geol. 24, 85–89.

Wilson, S.A., Ridley, W.I., Koenig, A.E., 2002. Development of sulfide calibration standards for laser ablation inductively-coupled mass spectrometry technique. J. Anal. At. Spectrom. 17, 406–409.